

**ASSOCIATION EURATOM - UNIVERSITY OF LATVIA
AEUL**



ANNUAL REPORT 2007



Edited by

Olgerts Dumbrajs

Institute of Solid State Physics University of Latvia

FOREWORD

A new era started in the European fusion research from 2007. Following the ratification of the ITER Agreement by all the Parties the International Organization came officially into being on 24th October. The first meeting of the ITER Council took place on 27th November. The preparation of the site in Cadarache has started with particular care being taken to minimise the environmental impact. The 7th Framework Programme was launched from the beginning of 2007. EURATOM Fusion Programme in FP7 provides a fair funding for fusion research in parallel with ITER construction. This is extremely important to keep Europe as the leader in the worldwide fusion research. On 27th March 2007, the Council of Ministers adopted the Statutes of the European Joint Undertaking for ITER and the Development of Fusion Energy, known as “Fusion for Energy (F4E)”, with its seat in Barcelona.

The Association EURATOM-University of Latvia (AEUL) has been active in the Physics and Technology areas.

In the Physics area, a significant programme has been continued in collaboration with the Association EURATOM-IST. A liquid metal jet for the tokamak ISTTOK was provided to study its possible application as a liquid metal limiter in a tokamak. This study was supported by relevant spectroscopy investigations. On the theory side the code for computations of mode competition in coaxial gyrotrons was further developed and two new of activities were launched: (i) theoretical studies of stochastization of magnetic fields and magnetic reconnection in tokamaks, (ii) investigations of irradiation stability of reactor materials.

In the Technology area the main activities were: (i) investigation of effects of the magnetic field, radiation and temperature on the tritium release from beryllium pebbles and on technologies for detritiation of beryllium materials, (ii) identification of chemical forms of tritium accumulated in the irradiated Be pebbles, (iii) development of a prototype of the radiation-hard capacitive bolometer assembly based on PZ ferroelectric material.

The Association programme is implemented mainly in collaborations with other Associations of the EURATOM fusion programme. The national financial support for the Association work is provided by the Ministry of Education and Science.

I would like to express my sincere thanks to all those who have assisted the progress of the Association EURATOM-University of Latvia, in particular: EURATOM officers; the staff of the EFDA close support units, the Ministry of Education and Science of Latvia, University of Latvia, members of the associated committees, the administrative staff of the Association, and last, but not least, the scientists and technicians who have been actively involved in the R&D programme of the Association.

Andris Sternberg
Head of the Research Unit
Association EURATOM-University of Latvia

Annual Report 2007

Association EURATOM-University of Latvia

FOREWORD	1
1. INTRODUCTION	4
2. FUSION PROGRAMME ORGANISATION	4
2.1 Programme Objectives	4
2.2 Association EURATOM-University of Latvia	4
2.3 Fusion Research Units	5
2.4 Association Steering Committee	5
2.5 National Steering Committee	5
2.6 The Latvian Members in the EU Fusion Committees	5
2.7 Public Information	6
2.8 Funding and Research Volume 2007	7
3. PHYSICS PROGRAMME – FUSION PHYSICS	7
3.1 Preparation of a Gallium multi-jet limiter for installation on tokamak ISTTOK	8
3.2 Investigation of metal ions in fusion plasmas using emission spectroscopy	14
3.3 Laser ablation spectroscopy for impurity depth profiling and concentration imaging in plasma facing materials	16
3.4 Theory and Code Development	18
4. EFDA FUSION TECHNOLOGY PROGRAMME	25
4.1 Magnetic field effect on technologies for detritiation of beryllium materials	25
4.2 Assessment of the effects of magnetic field, radiation and temperature on the tritium release from beryllium pebbles. Identification of chemical forms of tritium accumulated in the irradiated beryllium pebbles	30
4.3 Development of a prototype of the radiation – hard capacitive bolometer assembly based on ferroelectric material	35
5. STAFF MOBILITY ACTIONS	37

5.1 Staff Mobility Visits	37
6. OTHER ACTIVITIES	38
6.1 Conferences, Workshops and Meetings	38
6.2 Visits	38
6.3 Visitors	38
7. PUBLICATIONS 2007	38
7.1 Fusion Physics and Plasma Engineering	38
7.2 Fusion Technology	40
7.3 General Articles	41
7.4 Doctoral and Graduate Theses	41

1. INTRODUCTION

This Annual Report summarises the fusion research activities of the Latvian Research Unit of the Association EURATOM-University of Latvia in 2007.

The activities of the Research Unit are divided in the Fusion Physics Programme and Technology under the Contract of Association and Technology Programme under EFDA.

The Physics Programme is carried out at IP UL – Institute of Physics, University of Latvia, and at ISSP UL – Institute of Solid State Physics, University of Latvia. The research areas of the Physics Programme are:

- Preparation of a Gallium multi-jet limiter for installation on tokamak ISTTOK
- Investigation of metal ions in fusion plasmas using emission spectroscopy
- Theory and Code Development.

The Technology Programme is carried at ISSP UL and at ICP UL - Institute of Chemical Physics, University of Latvia. The technology research and development under EFDA is focused on:

- studies of the magnetic field effect on technologies for detritiation of beryllium materials
- assessment of the effects of magnetic field, radiation and temperature on the tritium release from beryllium pebbles
- identification of chemical forms of tritium accumulated in the irradiated beryllium pebbles
- development of a prototype of the radiation – hard capacitive bolometer assembly based on ferroelectric material.

Several Staff Mobility actions took place in 2007: to IPP Garching, FZK Karlsruhe , UKAEA Culham, and ISTOK Lisbon.

2. FUSION PROGRAMME ORGANIZATION

2.1 Programme Objectives

The Latvian Fusion Programme, under the Association EURATOM-University of Latvia, is fully integrated into the European Programme, which has set the long-term aim of the joint creation of prototype reactors for power stations to meet the needs of society: operational safety, environmental compatibility and economic viability. The objectives of the Latvian programme are: (i) to carry out high-level scientific and technological research in the field of nuclear fusion, (ii) to make a valuable and visible contribution to the European Fusion Programme and to the international ITER Project in our focus areas. This can be achieved by close collaboration with other Associations.

2.2 Association EURATOM-University of Latvia

The Latvian contribution to the European fusion programme began in 2000 in the form of cost-sharing actions (fixed contribution contracts with EURATOM). The Association

was established on 19 December 2001 incorporating the existing cost-sharing actions into its work plan.

2.3 Fusion Research Units

The Latvian Research Unit of the Association EURATOM-University of Latvia consists of three Institutes of University of Latvia.

1. IP UL – Institute of Physics, University of Latvia
32 Miera St., Salaspils LV-2169, Latvia.
Phone +371 6 7944700, Fax. +371 6 7901214
2. ISSP UL – Institute of Solid State Physics, University of Latvia
8 Kengaraga St., Riga LV-1063, Latvia.
Phone +371 6 7187810, Fax. +371 6 7132778
3. ICP UL - Institute of Chemical Physics, University of Latvia
4 Kronvalda Blvd., Riga LV-1010, Latvia.
Phone +371 6 7033884, Fax. +371 6 7033884

2.4 Association Steering Committee

The research activities of the Latvian Association EURATOM-University of Latvia are directed by the Steering Committee, which comprises the following members in 2007:

Mr. Douglas Bartlett, EU Commission, Research DG
Mr. Steven Booth, EU Commission, Research DG
Mr. Marc Pipeleers, EU Commission, Research DG

The Steering Committee had one meeting in 2007, at University of Latvia, on 25th April.

2.5 National Steering Committee

The national Steering Committee advises on the strategy and planning of the national research effort. It sets also priorities for the Latvian activities in the EU Fusion Programme. The national Steering Committee had the following members in 2007:

Mrs. Maija Bundule, Ministry of Education and Science
Mr. Ivars Lacis, University of Latvia
Mr. Andrejs Silins, Latvian Academy of Sciences

2.6 The Latvian Members in the EU Fusion Committees

Consultative Committee for the EURATOM Specific Research and Training Programme in the Field of Nuclear Energy-Fusion (CCE-FU)

Mr. Janis Berzins, ISSP UL
Mr. Andris Sternberg, ISSP UL

EFDA Steering Committee

Mr. Andris Sternberg, ISSP UL

Science and Technology Advisory Committee (STAC)

Mr. Olgerts Dumbrajs, ISSP UL

Mr. Andris Sternberg, ISSP UL

Governing Board for the Joint European Undertaking for ITER and the Development of Fusion Energy, "Fusion for Energy" (F4E GB)

Mrs. Maija Bundule, Ministry of Education and Science

Mr. Andris Sternberg, ISSP UL

EFDA Public Information Group

Mr. Maris Kundzins, ISSP UL

2.7 Public Information

Conferences

Results of fusion research were presented at:

- the annual scientific conference of University of Latvia,
- International Baltic Sea Regional Conference "Functional materials and nanotechnologies" (FM&NT 2007).

Exhibitions

Exposition and presentations during Career days at Riga Technical University.

Educational activities

Excursions at ISSP UL from schools two to three times a month, PhD students from Latvian universities. Booklets about ISSP UL and EFDA were distributed.

Television, press

Presentations in TV – popular science for students.

Booklet and a DVD video "ITER, the way to fusion" were distributed at universities and schools.

EFDA Steering Committee meeting

EFDA Steering Committee meeting took place at ISSP UL, 25th -26th October

Workshop

CONNECT Latvia network breakfast on 30th November at ISSP UL with presentations and excursions.

Scientific cafeteria

In the main building of University of Latvia with presentations and discussions about the problems of the future power industry.

2.8 Funding and Research Volume 2007

In 2007, the expenditure of the Association EURATOM-University of Latvia was about 526 459.00 EUR, including Staff Mobility actions

Item	Expenditure (EUR)
General Support (20% EU contribution)	431 594.00
Physics	431 594.00
Underlying Technology	0.00
Technology Tasks EFDA Art. 5.1.a (20% EU contribution)	84 761.00
Missions and Secondments under the Agreement on Staff Mobility (100% EU contribution)	10 104.00
TOTAL	526 459.00
Priority Actions (Additional 20% EU contribution)	0.00
Collaborative Actions (Additional 20% EU contribution)	501 076.00

3. PHYSICS PROGRAMME – FUSION PHYSICS

The fusion physics work has been performed at two institutes in very close co-operation with other EURATOM Associations, in particular EURATOM-IST, Portugal, EURATOM-ENEA, Italy, EURATOM IPP, Germany, and EURATOM- FZK, Germany.

Institute: **IP UL – Institute of Physics, University of Latvia**

Research scientists: Dr. Imants Buceniaks
Dr. Janis Freibergs
Dr. Agris Gailitis
Dr. Olgerts Lielausis
Dr. Arturs Mikelsons
Dr. Eriks Platacis
Dr. Alberts Romancuks
Dr. Anatolijs Ziks

Institute: **ISSP UL – Institute of Solid State Physics, University of Latvia**

Research scientists: Dr. Olgerts Dumbrajs
Dr. Aleksejs Gopejenko
Dr. Jevgenijs Kotomins
Dr. Vladimirs Kuzovkovs
PhD. Anatolijs Sarakovskis
Dr. Andris Sternberg
Dr. Ivars Tale
Dr. Vismants Zauls
Dr. Jurijs Zhukovskis
Dr. Guntars Zvejnieks

3.1 Preparation of a gallium multi-jet limiter for installation on tokamak ISTTOK

Principal investigator E. Platacis

3.1.1 Initial conditions for the development of a multi-jet limiter for ISTTOK

The idea of the transfer to a multi-jet limiter is clear – to organize an approximately 1 cm wide opaque obstacle able to “scrape off” a real outer layer of the plasma. Under such conditions, in contrast to the single jet case, a noticeable influence of the limiter on the parameters of discharge can be expected. To make the transfer as easy as possible it was decided to keep the main parameters of the stands (both on ISTTOK and at IP UL) unchanged and to concentrate on changes of the injecting part, starting with the outlet flange of the upper reservoir and following down to the nozzles (Fig. 3.1.1.1).

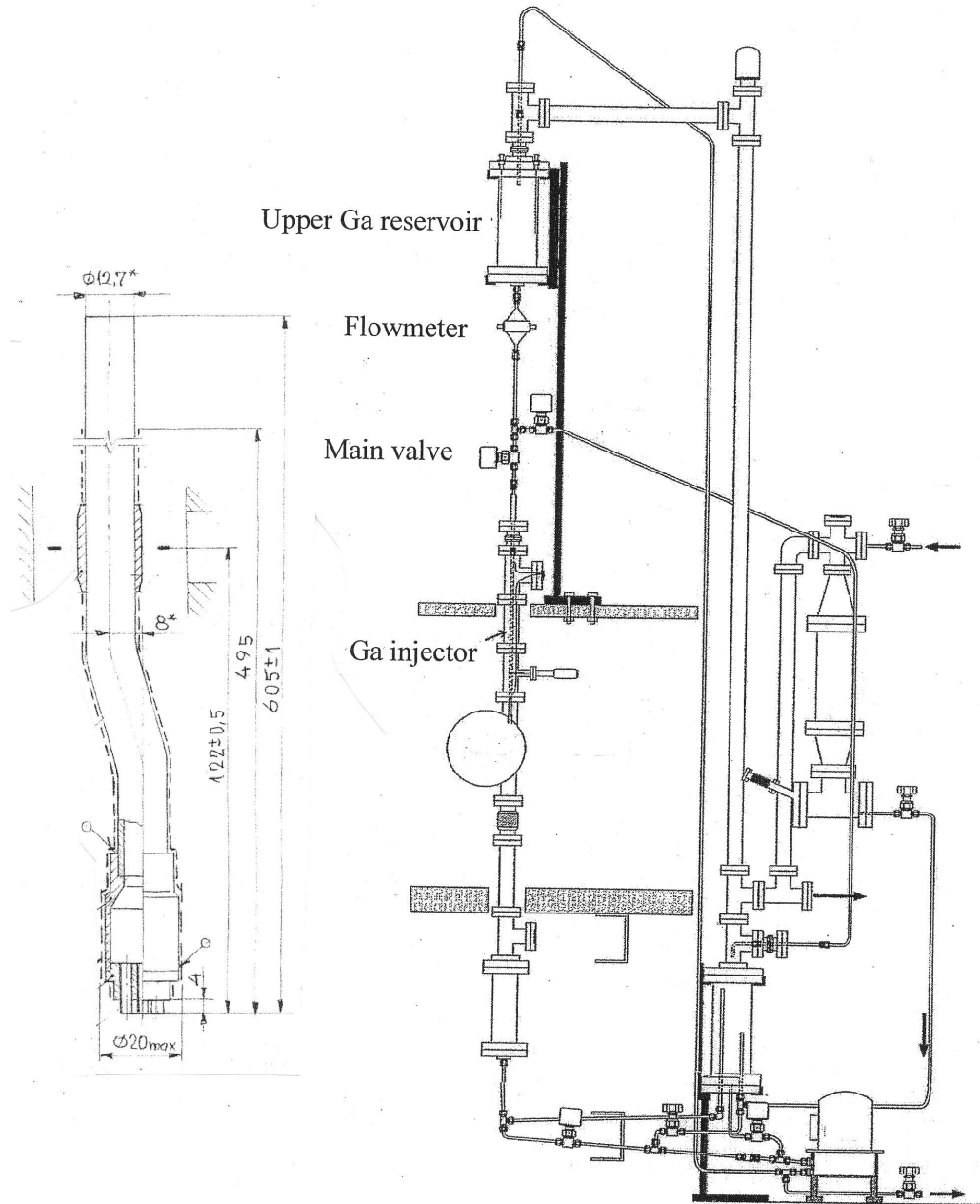


Figure 3.1.1.1 Scheme of Ga limiter installed on ISTTOK

On the left hand side of the figure the newly developed unit is shown with the nozzles shifted closer to the wall of the inlet opening. The proposal of a shifted injector must be considered as typical especially for multi-jet systems. In the single jet version the nozzle was placed directly above the centre of the $d=38$ mm outlet port of the chamber. If the single jet (d of order 2.5mm) would be directly replaced by a multi-jet screen (d of order 10mm) we would risk that for regular discharges the cross section is too strongly limited. Therefore it was proposed to shift the nozzle section of the injector as close as possible to outer edge of the $d=38$ mm inlet port and then step by step to push it deeper into the volume, using a similar positioning mechanism as in the case of the single jet. However in such a situation it may happen that the jets can be targeted against the outer edge of the outlet port.

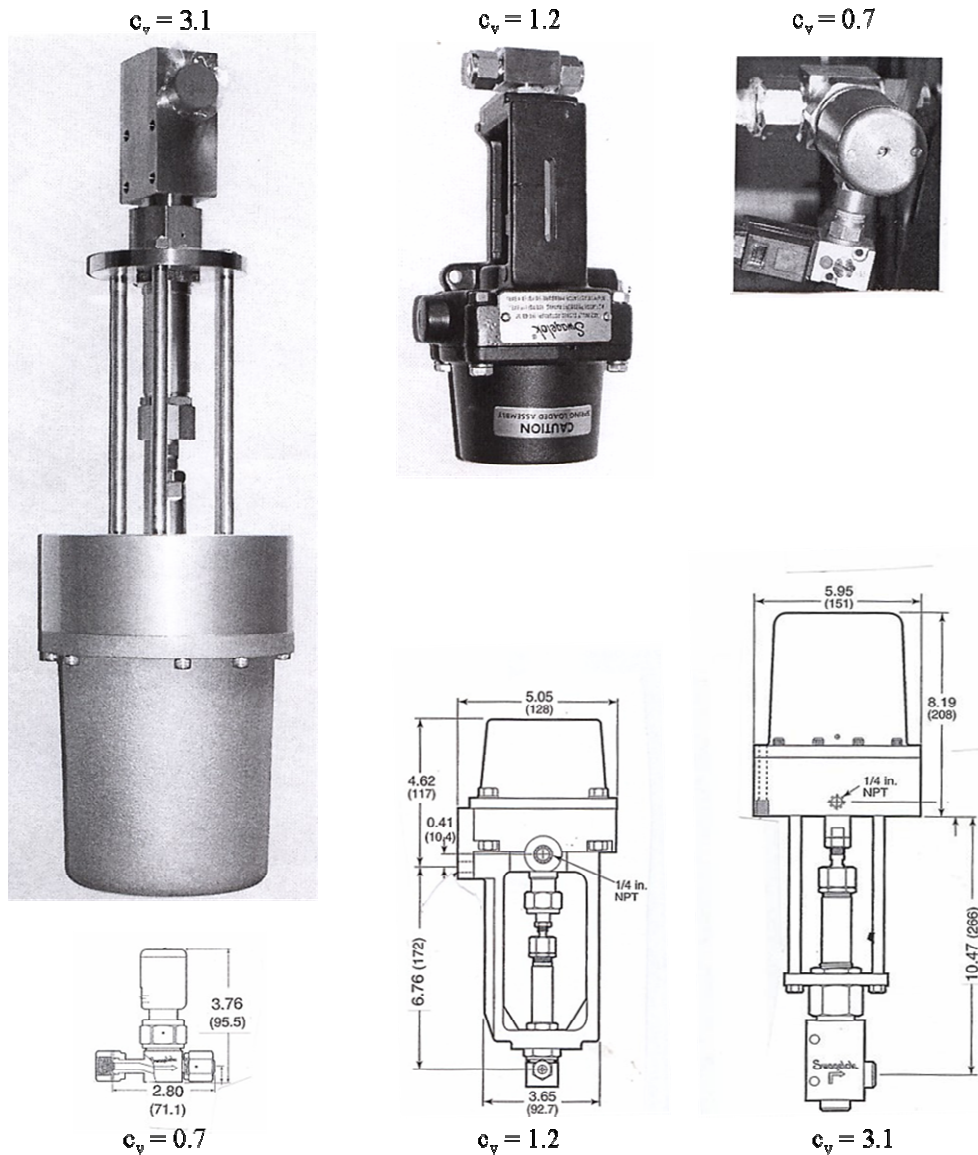


Figure 3.1.1.2. Bellow sealed valves

Other difficulties are related to the fact that at the same acting pressure $\Delta h= 1.3$ m the flow-rate must be increased three, four or even five times (depending on the number of jets in the multi-jet system) compared with the initial single-jet version. To reach the same breakup length for the multi-jet system the velocity in each of the jets must remain unchanged, equal to the velocity of the single-jet version. The first and simplest pressure consumer, are hydraulic losses in the connecting tubes. Their minimization was

not even considered, the diameter of the tubes was simply increased from $d=5\text{mm}$ to $d=10\text{ mm}$. As next, local losses in the “on/off” shutting valve were analyzed. Here unexpected problems occurred. It turned out that the choice of available bellows sealed valves is very limited, at least at the *Swagelok Company*. In addition, in the transfer to lower hydraulic resistances the size of the valves is critically increasing (Fig. 3.1.1.2).

The ratio between the flow-rate and pressure drop in the valve is characterized by the flow coefficient c_v : $q = c_v \Delta p^{1/2}$. The numerical values of c_v presented in Fig. 3.1.1.2 correspond to q measured in “gal/min” and Δp measured in “psi”. In the single jet version it was possible to use a small valve with $c_v=0.36$. Approximately the same dimensions (height of order 100 mm) are characteristic also for the valve with $c_v=0.7$ (Fig. 3.1.1.2). It was decided to build the multi-jet injector on the basis of this BN8 size valve. However, in such a case only a three jet version can be proposed, as discussed below. Four jets are requiring already an 8UW series valve with $c_v= 1.2$. The dimensions of this valve remain acceptable, the height = 290 mm. It should be remembered, that the valve must be mounted on a $d=12\text{ mm}$ tube. Just a four jet version with such a valve was taken as the basis for further development. However initially it was proposed to install on ISTTOK a limiter with a higher number of jets. In direct measurements it was found that in such a case a valve with a higher flow coefficient is required. Next after series 8UW, follows series 12UW, and these “machines” are huge indeed, reaching in height 465 mm. Also such a valve was acquired (see Fig. 3.1.1.2), but turned out to be unacceptable for installation on a $d=12\text{ mm}$ tube, at least during the first phase of investigations. At the same time it should be remembered that this valve is designed with 16 mm in/out joints, i.e., not so big.

Finally, the jets are pulled out with a definite non-zero velocity and the corresponding accelerating energy, again generated by the same pressure, is lost for the system. Such outlet pressure losses are present in all “open” hydraulic systems, but their relative role can be very different. In Fig. 3.1.1.3 a specific case is illustrated.

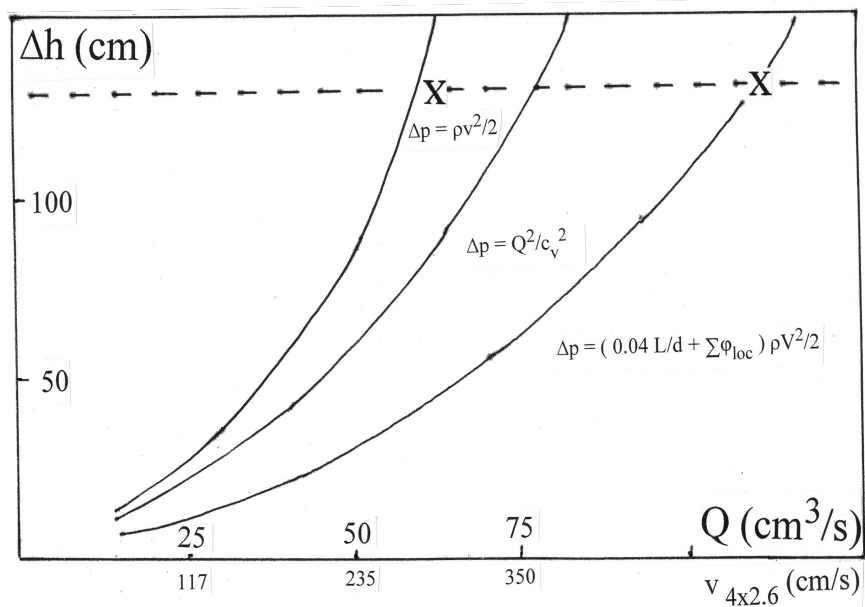


Figure 3.1.1.3 Hydraulic scheme for determination of the jet velocity

It can be seen that our configuration is rather “open,” the pressure losses in all the three mentioned elements (connections-valve-outlet) are practically equal. Curve 1 represents losses in an “empty” connection, without flow meter and valve. For the operating value

of the hydraulic height $\Delta h = 130$ cm (see Fig. 3.1.1.3) the corresponding flow-rate Q was directly measured and the curve was drawn through this point. Curve 2 corresponds to the situation when the mentioned valve with $c_v=1.2$ was included in the hydraulic chain. Losses calculated from the relation $Q = c_v (\Delta p)^{1/2}$ were simply added to curve 1. To determine the outlet losses, it is necessary to know the outlet velocity. A case with four $d=2.5$ mm jets was considered, the value of velocity in each of such jets is also shown along the x-coordinate. The outlet losses were determined by means of the relation $\Delta h = v^2/2g$. To construct the curve 3, these outlet losses were added to curve 2. For the system “connections-valve” at the acting pressure the flow-rate was also directly measured, $Q = 60$ cm³/s was reached. Probably by accident for such a simplified scheme, but this value corresponds to the independently constructed curve 3. A similar approach can be applied also in cases with different number of jets, their diameters, as well as, with different characteristics of the valve. Let us take an example. Considering the potential application to FTU, because of space limitations, only a small valve with $c_v=0.7$ can be proposed. At $\Delta H=130$ cm for a single $d=3$ mm jet calculations were predicting velocity $v=3.8$ m/s, while in the experiment $v=4.4$ m/s was reached. In this most complicated case, the outlet losses were clearly prevailing, reaching 75% of the total pressure losses.

3.1.2. Behaviour of individual jets in multi-jet injectors

The previous section leads to the conclusion that in systems under consideration the main working parameter - the velocity of the jets - can be estimated or predicted with a sufficient accuracy. Moreover, this accuracy can be increased, first of all, by using more accurate expressions for the mentioned losses. In the case of a single jet it would be acceptable to determine the second main parameter, the breakup length. However, it turns out that in a real design of a multi-jet injector the individual jets do not behave as nicely as initially expected. Initial experiments performed in 2006 confirmed that all jets in a three jet system break up according to the rules established for an individual jet (Fig. 3.1.2.1).

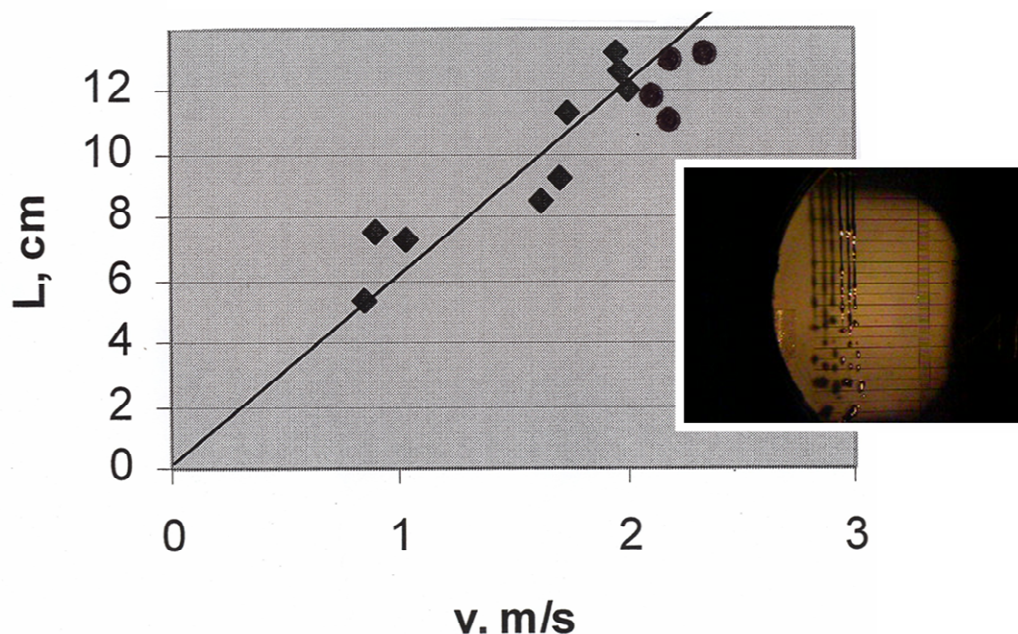


Figure 3.1.2.1. Break-up length in the system of three $d=2.5$ mm InGaSn jets

However, in this case the nozzles were placed with sufficient spacing, determined in special measurements. By means of a precise mechanism two jets were brought closer and closer and it was found that 13 cm long jets behave as individuals down to a distance of approximately 2.5 mm. However, in a real design it is difficult to take all these requirements fully into account. For example, spacing becomes strongly limited, because of the necessity to bring the nozzles as close as possible to the outer wall of the inlet opening (see Fig. 3.1.1.1). All nozzles must be squeezed in outer $d \approx 1$ cm housing. In reality the breakup length in a multi-jet system can differ significantly from the ideal “single jet” case. An example is presented in Fig. 3.1.2.2 where the breakup length in a system of four jets can be seen ($d=2.6$ mm; $v=2.8$ m/s).

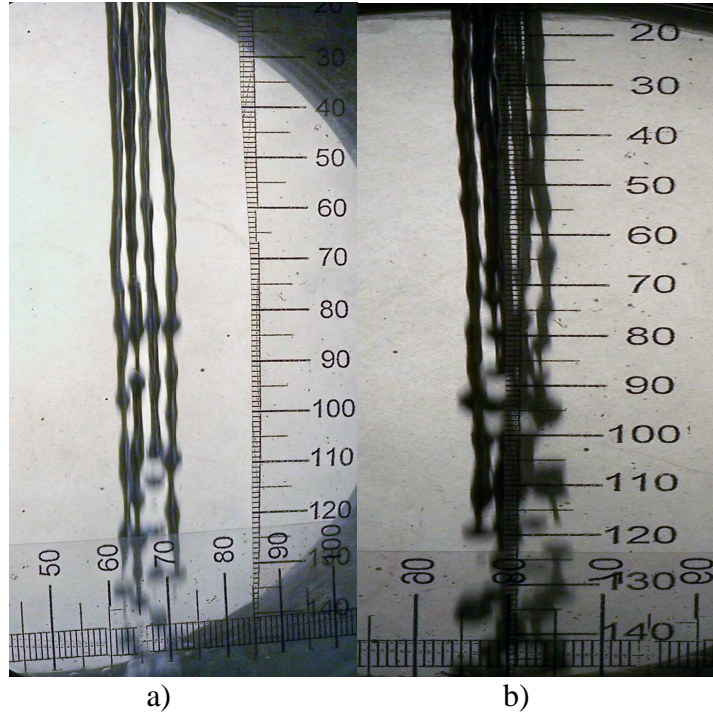


Figure 3.1.2.2 a) Version proposed for installation on ISTTOK: four $d=2.6$ mm jets; BUL ~ 11 cm; $v = 2.80$ m/s; b) version with five $d=2.6$ mm jets; BUL ~ 9 cm; $v = 2.3$ m/s. Photo has been taken under the angle when all jets can be clearly seen. Scales are given both for the break-up length and the side deviation

According to the “single jet” predictions BUL= 21 cm should be expected, in reality BUL of order 11 cm was reached, i.e. almost two times shorter.

3.1.3 Water as a modelling liquid for investigation of the Rayleigh instability in liquid metals

In the proposal under consideration the MHD interaction (generation of induced currents) should be avoided due to the Rayleigh instability – breakup of liquid jets in shorter/smaller fractions. This process is governed by the Weber number Wb . The breakup length L for a jet of the diameter d can be determined by means of a rather simple expression

$$L/d = \text{coef.} (Wb)^{1/2} = \text{coef.} (\rho v^2 d / \sigma)^{1/2},$$

where ρ is density, σ is surface tension, and v is velocity.

For a rather wide range of quasi-similar conditions *coef.* remains practically constant, weakly dependent on the Reynolds number Re . In the reference period a physically interesting and practically important result was achieved. Namely, it has been experimentally confirmed that the initial formal assumption that the ordinary water can be used for modelling the breakup process in liquid metals of interest for us is correct. This is so because for water and such materials as InGaSn and Ga for given velocity v and diameter d the values of the Weber number (and also of the Reynolds number) differ very little:

$$\begin{aligned} \text{Wb}(\text{InGaSn}) / \text{Wb}(\text{H}_2\text{O}) &= 1.28; & \text{Re}(\text{InGaSn}) / \text{Re}(\text{H}_2\text{O}) &= 2.5 \\ \text{Wb}(\text{Ga}) / \text{Wb}(\text{H}_2\text{O}) &= 0.66; & \text{Re}(\text{Ga}) / \text{Re}(\text{H}_2\text{O}) &= 3.3 \end{aligned}$$

for parameters

$$\begin{aligned} \text{InGaSn} & \quad (\rho = 6400 \text{ kg/m}^3; \sigma = 0.353 \text{ N/m}; \nu = 4 \cdot 10^{-7} \text{ m}^2/\text{s}) \\ \text{Ga} & \quad (\rho = 6093 \text{ kg/m}^3; \sigma = 0.723 \text{ N/m}; \nu = 3 \cdot 10^{-7} \text{ m}^2/\text{s}) \\ \text{H}_2\text{O} & \quad (\rho = 1000 \text{ kg/m}^3; \sigma = 0.072 \text{ N/m}; \nu = 10 \cdot 10^{-7} \text{ m}^2/\text{s}) \end{aligned}$$

In Fig. 3.1.3.1 the results are compared when the relative breakup length L/d has been measured both for the liquid metal and the water.

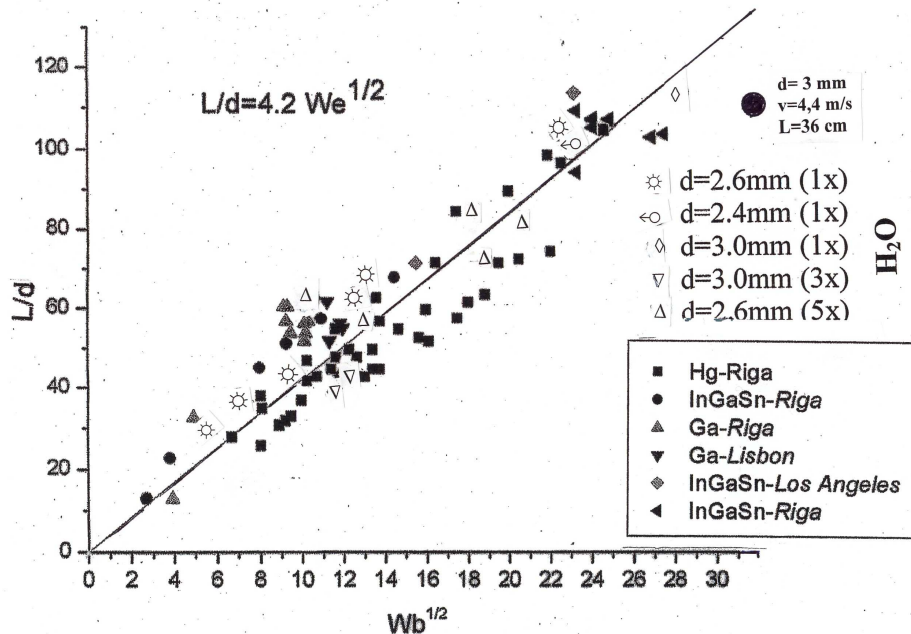


Figure 3.1.3.1 Break-up length of the liquid metal and the water jets are practically the same, both for H_2O and InGaSn

The „old” points marked black were used to derive a very convenient formula for liquid metals

$$L/d = 4.2 (\text{Wb})^{1/2}.$$

The empty points correspond to measurements with water. Both sets of measurements agree with each other surprisingly well. This means that in general the underlying physical mechanism practically depends on only one dimensionless parameter, the Weber number.

The results of the significantly more convenient measurements with water can be used also for the discussion about the reasons for the “strange” behaviour of individual jets in liquid metal multi-jet systems. Measurements with water confirm that breakup length for individual jets in a multi-jet system can remain practically unchanged compared with the single jet case. Both for individual jets (1x), and for ensembles of three (3x) and five (5x) jets the breakup length depends on the Weber number in the same manner.

It should be emphasized that the geometry of the nozzle units in the two cases was kept practically the same, both for H₂O and InGaSn.

3.2 Investigation of metal ions in fusion plasmas using emission spectroscopy

Principal investigator I. Tale

3.2.1 Investigation of single and multiple ionized Ga atoms in the tokamak plasma

The following experimental setup (Fig. 3.2.1.1) present at ISTTOK was used for obtaining spectral and spatial information of the plasma.

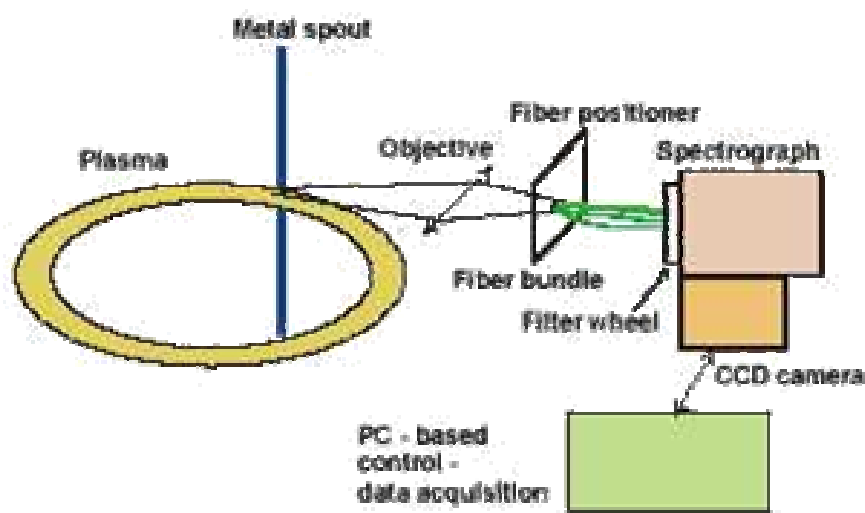


Figure 3.2.1.1 Experimental set-up

Owing to its privileged viewing area with respect to the observation of the light emitted during plasma-liquid metal interaction, the tokamak port has been used to place the collection optics for a multi-channel (7 viewing points in a radial direction) optical fiber relaying radiation to a ½ m imaging monochromator (CVI laser DK480). This apparatus is equipped with a triple-grating turret system, blazed at 300, 500 and 750 nm and 1200 gr/mm each. A spectroscopic CCD (Spectral Products SPH5) camera at the output focal plane of the spectrometer allows the acquisition of line intensities emitted from the plasma in the 200 to 900 nm spectral region. During each discharge it was possible to obtain 4 spectra corresponding to 4 viewing lines of sight radially distributed (due to the magnification ratio of the spectrometer to fiber coupling optics, three end channels of the fiber were lost), and focused on the liquid metal jet poloidal plane where it covers 1.2 cm span. The main advantage of this diagnostic was a clear identification of the presence of gallium (both neutral and ion species) in the plasma.

Fig. 3.2.1.2 a) illustrates a spectrum that shows the characteristic lines of neutral gallium at 417.2 and 403.3 nm. In the same figure it is also possible to identify a few spectral lines produced by gallium ions (both Ga⁺ and Ga²⁺). The analysis of the mentioned spectra, acquired during a shot by shot spatial scan of the plasma, provided additional information about the neutral and the ion relative distribution in the radial direction. The results are presented in Fig. 3.2.1.2 b). As expected, the maximum emission for the neutral gallium is seen in the vicinity of the jet position while species of higher degrees of ionization penetrate deeper into the plasma owing to the radial diffusion. In practice, since viewing is done along the toroidal direction and ions are

transported along the magnetic field lines, it should be pointed out that the observed distribution is broadened with respect to the real one. The maximum intensities in the emission profiles are close to each other due to the low ionization potential for the gallium ions (6, 20.5 and 30.7 eV for GaI, II and III, respectively).

The procedure used in the blue region of the spectra has been repeated in the red region, since several other lines are available for this study ($\lambda_{\text{GaI}}=639.7$ nm, $\lambda_{\text{GaII}}=633.4$ nm and $\lambda_{\text{GaIII}}=599.4$ nm). It is important to emphasize that in the case of absence of the liquid metal jet in the chamber, no traces of gallium lines (within the sensitivity of the CCD camera) were observed. In spite of having the data of line intensities, it was not possible to obtain density values for the liquid metal penetrating the plasma, because no absolute calibration has been performed.

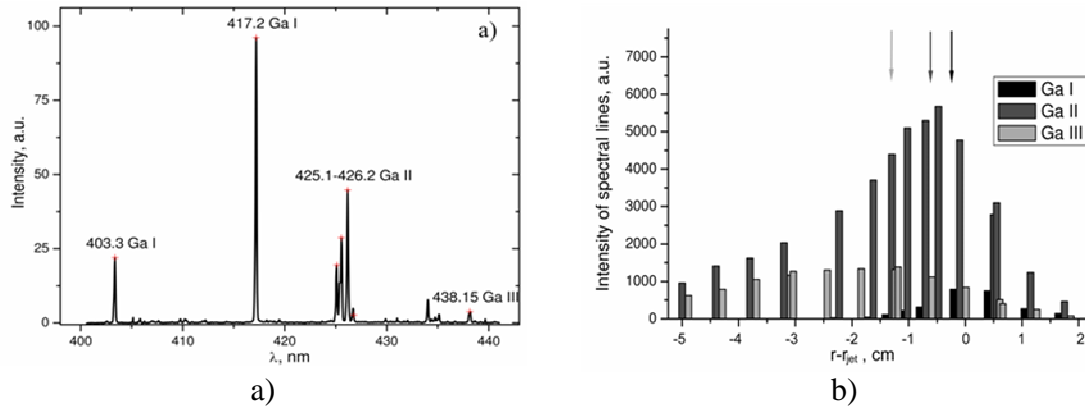


Figure 3.2.1.2 a) characteristic spectrum of gallium, b) distribution of spectral lines in ISTTOK plasma. The arrows indicate the maximum emission position

3.2.2. Modification of the spectroscopic system

A new design of the light accepting optics concerning modification of the optical fiber is proposed (Fig. 3.2.2.1). It was mentioned before that only four fibers of possible seven ones were used to perform the scan of the poloidal plane of the tokamak. This was due to geometric amplification of the exit signal at the fiber end. This problem will be solved by a new fiber, which will allow us to perform both the stationary and the time-resolved spectroscopic measurements of the ISTTOK plasma. The entrance end of the fiber consists of two rows of totally 2×15 fibers. The row at the exit end is devoted to the stationary spatially resolved measurements. The other row of 15 fibers is divided into three bundles with five fibers each, suitable for coupling to photomultiplier tubes (PMT). Subsequently PMTs will be connected to an oscilloscope enabling registration of time resolved signals from three different regions in the poloidal plane.

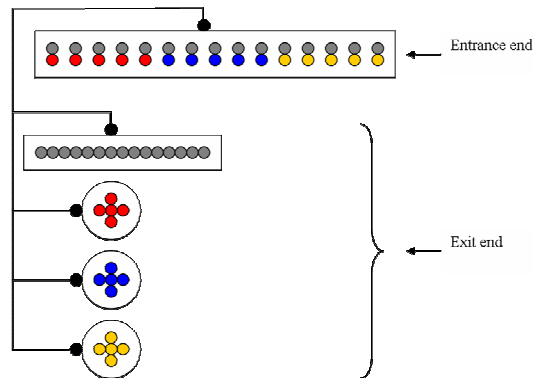


Figure 3.2.2.1. Optical fiber system

3.3 Laser ablation spectroscopy for impurity depth profiling and concentration imaging in plasma facing materials

Principal investigator I. Tale

Laser-induced plasma spectroscopy of the samples cut from the ASDEX Upgrade inner wall tiles after being in contact with tokamak plasma was carried out. As the laser-induced plasma source, a 1064 nm Q-switched Nd:YAG laser operating with 250 mJ pulse energy, 135 ps pulse width and 10 Hz pulse repetition rate was used. The spectrum of graphite R6710 target containing no impurities was recorded as a reference. As the main impurities of the AUG samples are tungsten and boron (might appear after the boronization of plasma-facing components), the graphite R6710 substrates sputtered with tungsten and boron carbide layers were also used as a reference.

To find the most convenient regime of ablation, 1 to 10 laser pulses at the pulse energies of 2, 5, 10 and 15 mJ were applied on each sample. For each pulse energy, 10 pulses gave the maximal information on the composition of the sample (fig.3.3.1). Comparing spectra obtained after the series of 10 laser pulses at different pulse energies (fig.3.3.2), the pulse of 15 mJ found to be the most informative. Increased pulse energy resulted in the formation of excessively deep craters and removal of the most informative layer with the first pulses.

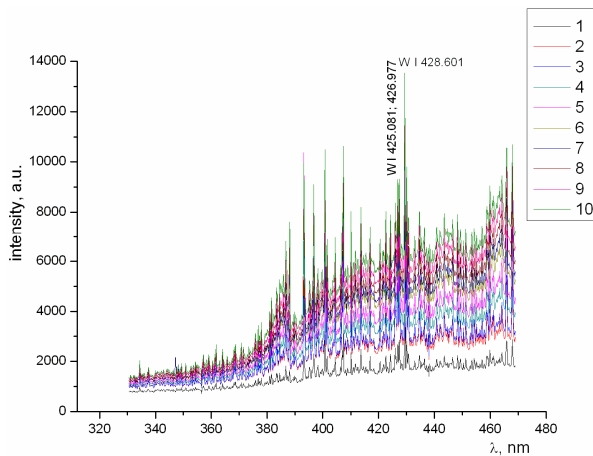


Figure 3.3.1. Laser-induced plasma emission spectra of W sputtered R6710 graphite sample. Numbers correspond to the number of pulses applied to the same spot at pulse energy of 10 mJ. C lines are not specified

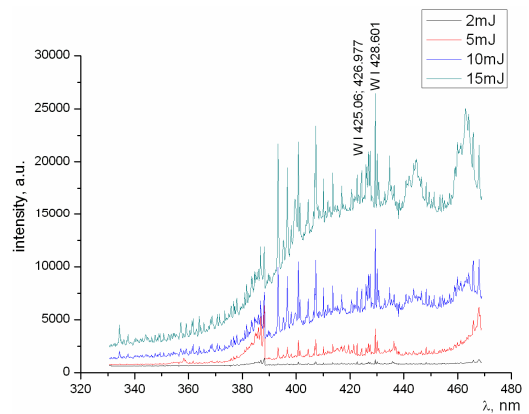


Figure 3.3.2. Spectra of the W sputtered R6710 graphite sample. 10 laser pulses at pulse energies from 2 to 15 mJ were applied. C lines are not specified

Figures 3.3.1 and 3.3.2 show the results for the tungsten sputtered R6710 graphite sample, but the experiments exhibit a common tendency for the all tested samples. In this regime, the ablation rate was about 70 nm for W and B₄C sputtered targets, while for the AUG sample it was around 0.5 μm . This is probably due to the different reflectance of the materials.

Figure 3.3.3 shows the comparison of the spectra of the reference samples and the AUG sample to identify the basic impurities (tungsten and boron). Apart from them, Fe I 390.294 nm and D _{α} 656.285 nm lines were identified. The source of Fe line might be the stainless steel components which are not shielded from the plasma.

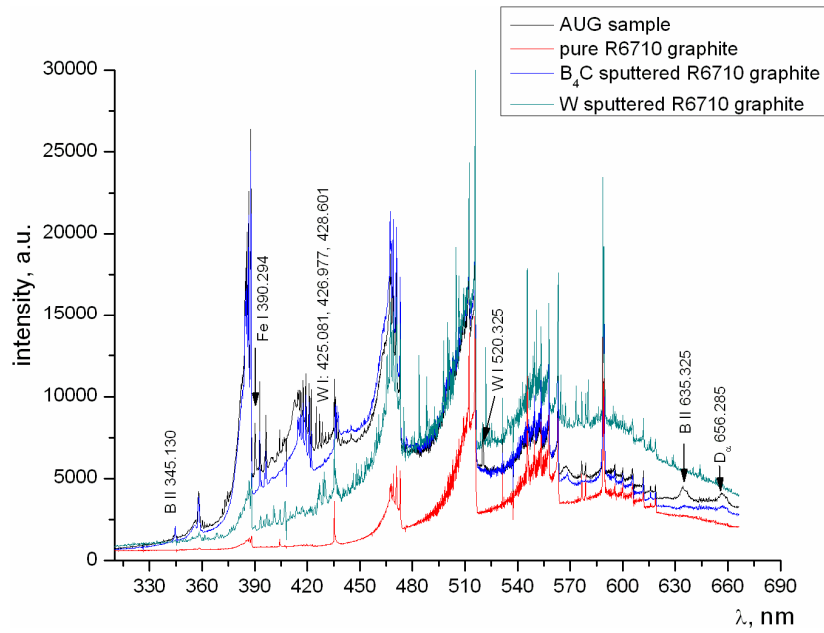


Figure 3.3.3 Spectra of reference and ASDEX Upgrade samples. Carbon lines are not specified in the figure

To follow the evolution of the appearance of deuterium line in the spectrum, signals in the spectral window of 580-680 nm were recorded. Fig. 3.3.4 represents spectra corresponding to the 1st, the 2nd, the 3rd, the 5th and the 10th consecutive laser pulses applied at the same spot of the sample.

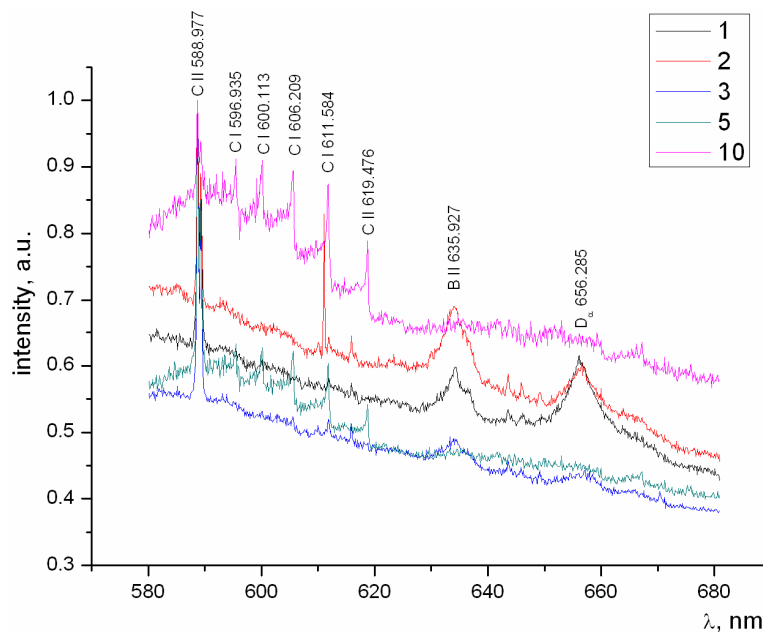


Figure 3.3.4. Evolution of D_{α} 656.285 nm line. The numbers correspond to the number of the pulse in the sequence

In the beginning of the ablation process, the intensities of the spectral lines of deuterium and boron are higher than those of the carbon. The relative intensities of spectral lines corresponding to the impurities and carbon change drastically when the number of laser pulses applied to the same spot increases. The signal of the substrate of the ASDEX Upgrade target does not change or increases. The first pulses show only the most

intense CII 588.977 nm line, while the other C I-II lines start to appear after the end of the 5th pulse.

3.4 Theory and Code Development

Principal investigator O. Dumbrajs

3.4.1 Mode competition in the 170 GHz coaxial cavity gyrotron for ITER

In gyrotrons with coaxial cavities mode competition is less severe than in ordinary gyrotrons. Nevertheless it remains a challenge both for theoreticians and experimentalists because there are significant discrepancies between the experimental results and the theoretical predictions. While experimental data obtained in high power high frequency coaxial gyrotrons for fusion are very scarce, there exist in the gyrotron community at least four codes with different level of sophistication which can be used for studies of mode competition in coaxial gyrotrons.

The code developed at the Helsinki University of Technology (HUT) and at ISSP LU is a self-consistent time-dependent code in which the voltage is increased stepwise after a stationary state is reached for a given voltage. This code allows one to take into account the following effects: i) electron velocity spread, ii) finite width of the electron beam, iii) reflections, iv) competition of two opposite rotations of one and the same mode, v) variable longitudinal depth of insert corrugations, vi) nonuniform magnetic field, vii) hysteresis of oscillations.

The code developed at the Forschungszentrum Karlsruhe (FZK) also is a self-consistent time-dependent code but with a continuous voltage increase. From the above-mentioned effects the code allows only for i) electron velocity spread.

The code developed at the National Technical University of Athens (NTUA) is a time-dependent, cold-cavity approximation code in which the voltage is increased either stepwise after a stationary state is reached for a given voltage, or continuously. The code allows for electron energy spread as well as all the above-mentioned effects, apart from iii) and v).

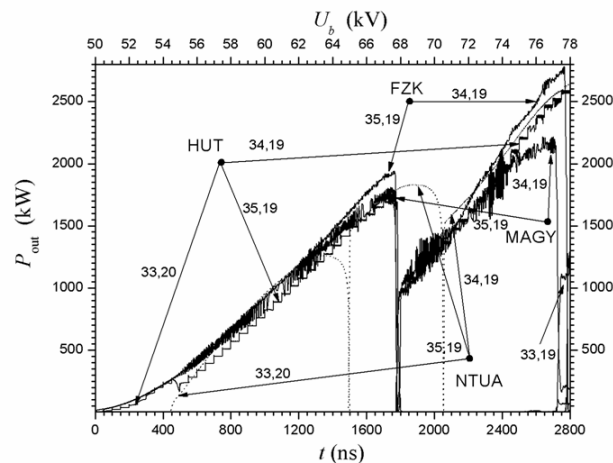


Figure 3.4.1.1. Mode competition scenarios predicted by the codes: HUT (ISSP UL), FZK, NTUA, and MAGY.

The gyrotron design code developed at the University of Maryland (UMD), Naval Research Laboratory (NRL) and Science Applications International Corporation (SAIC), USA is called MAGY. MAGY has been extended recently to be able to simulate mode competition in coaxial gyrotrons with corrugated inner insert. MAGY

provides self-consistent time-dependent solution of Maxwell Equations together with fully relativistic 3D equations of electron motion for an arbitrary voltage rise. The results of the calculations are presented in Fig.3.4.1.1.

Unfortunately the predictions of all four codes disagree with experimental observations according to which the gyrotron does not oscillate either in the $TE_{33,20}$, or in the $TE_{35,19}$ mode. It oscillates in the operating $TE_{34,19}$ mode until 72 kV with the output power of only about 1 MW. At higher voltages the $TE_{33,19}$ mode appears.

The reasons for these discrepancies are not known. However it should be emphasized that all the calculations presented here have been done without allowance for the various effects mentioned above. Further studies are needed.

3.4.2 Stochastization of magnetic fields and magnetic reconnection

The task is devoted to a systematic study of a sawtooth crash at ASDEX Upgrade tokamak. Sawtooth oscillations are periodic relaxation process of the plasma temperature, density and other plasma parameters in the central region of a tokamak. We employ the stochasticity hypothesis to explain the sawtooth phenomenon without a full reconnection assuming the interaction of the (1,1) mode with other periodicities and utilizing the Hamiltonian formalism with mapping technique. Main results can be summarized as follows.

- We demonstrate that stochastization appears due to the excitation of low-order resonances which are present in the corresponding safety factor profiles inside the $q=1$ surface which reflects the key role of the q_0 value. We show that the central safety factor is always less than unity in the case of a non-complete sawtooth reconnection.
- We determine heat diffusion coefficients in a stochastic magnetic field and reconstruct the amplitude drop during the crash phase. The assumed dynamics of the crash event is shown in Figure 3.4.2.1.

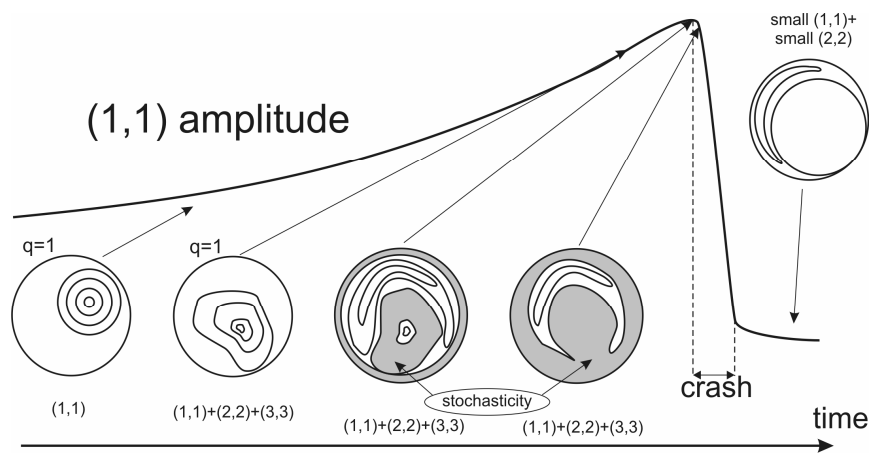


Figure 3.4.2.1 Artist's view of the temporal evolution of a sawtooth crash

In the first phase, the (1,1) mode grows alone. Higher harmonics appear close to the crash phase and destroy the symmetrical $m = 1$ structure of the mode without causing stochastization for which reconnection is needed to destroy the $q = 1$ surface. This occurs at the top of the mode amplitude leading to stochastization of the internal region and to decrease of the central temperature. As the starting time of the crash event we assume the time moment at which heat begins to flow intensively through the X-point

of the (1,1) island outside the $q=1$ resonant surface which corresponds to the drop of the plasma temperature and can be deduced from SXR measurements. The crash is regarded to be fait accompli at the time moment when the temperature becomes almost flat in the centre. Here the size of the (1,1) reduces to a stationary post-crash value and the heat channel at the X-point closes again which is shown as the final phase in figure 8. The 2D ECE measurements show deformation of the internal region inside the $q=1$ surface just before the crash which can be interpreted as an influence of the higher harmonics on the (1,1) mode. Subsequently the deformed mode several times tries to break the $q=1$ surface until a fast crash occurs.

- We demonstrate that during the pre-crash phase quasiperiodic transition to chaos occurs. Consistent with the most energetically favourable transition from quasiperiodicity to chaos, their frequency ratio is close to the conjugate golden ratio $G = f_2/f_1 = (\sqrt{5}-1)/2 \approx 0.618$ (Figure 3.4.2.2).

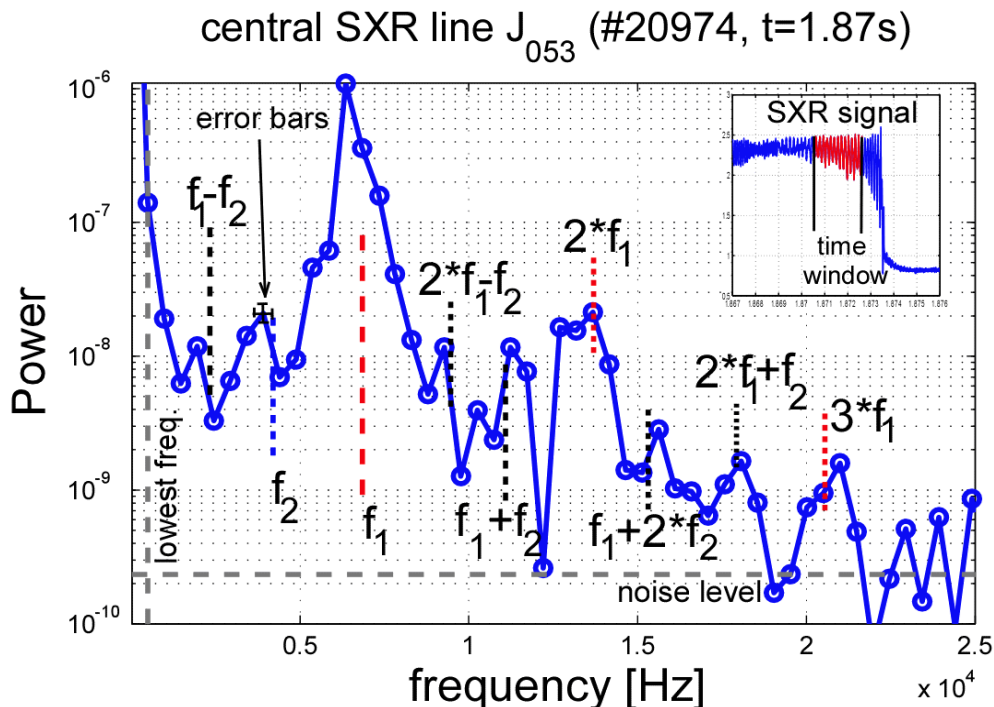


Figure 3.4.2.2. Power spectrum in the slightly quasiperiodic stage before the sawtooth crash

The low frequency part of the spectrum consists only of two frequencies ($f_1 = 6.59\text{kHz}$ and $f_2 = 3.93\text{kHz}$, $f_2/f_1 = 0.596 \pm 0.022$) and their linear combinations. The ratio between the primary frequencies is equal to the golden mean. (The lowest resolvable frequency in this case is 488Hz.) The Soft X-ray signal is shown in a small figure. We think that a sawtooth crash has a universal stochastic character and is closely related to enhanced transport by magnetic stochasticity.

We report on the accuracy of the Hamiltonian continuous time models by considering the mapping technique derived from Hamilton-Jacobi equation. The optimum time stepping in some models for the study of magnetic field in tokamaks is determined by using local criteria. A special attention is given to the analysis of the stochasticity produced by the time discretization.

3.4.3 Radiation stability of reactor materials

Principal investigator E. Kotomins

3.4.3.1. Objectives

In recent years, oxide-dispersion strengthened steels (ODS) are commonly considered as promising structural materials for fusion reactors. Excellent mechanical properties of ODS materials were achieved by introduction of a homogeneously distributed nano-scale Y_2O_3 -particles in the steel matrix (Figure 3.4.3.1.1). ODS steels are produced by mechanical alloying for several tens of hours followed by hot isostatic pressing at temperature around 1000-1200°C and pressure ~100 MPa (when iron matrix possesses a face-centred cubic γ -Fe lattice). Further improvement of mechanical properties and radiation resistance of ODS steels requires detailed understanding of oxide particle formation at atomic level.

The aim of our theoretical study was to perform the first principles modelling of ODS steels in order to predict and control in the future their radiation and mechanical properties.

3.4.2.2 Introduction

The recent experimental findings indicate that the picture of oxide particle formation is still not clear. Oxide particles found after hipping are the remnants of the initial yttrium oxide powder crushed by mechanical alloying (MA) incorporated into steel matrix. This view is supported by the fact that the hipping temperature is much lower than the melting temperature of yttria ($T_m \sim 2410^\circ\text{C}$) and therefore any thermal processes of oxide particle transformation should be excluded.

There are also evidences that after the milling at least a part of Y and O atoms resides in the solid solution. In such a case, the formation of oxide particles can occur at the hipping stage as a result of Y-O co-precipitation where precipitation kinetics is governing the process of oxide particles formation. Experimentally, ODS particles were found to be partly coherent with the surrounding ferrite matrix:

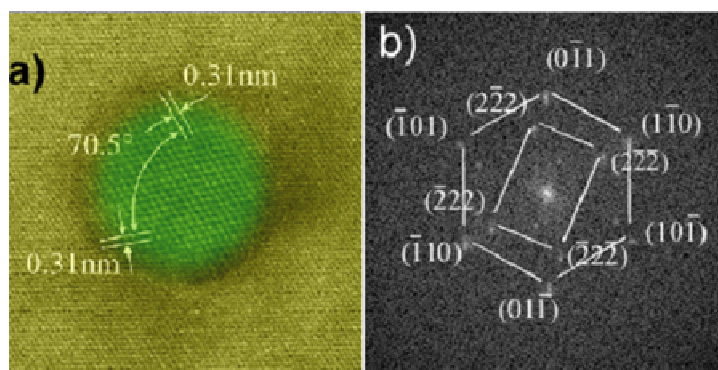


Figure 3.4.3.1.1 HRTEM micrograph of Y_2O_3 nanoparticle embedded into ferrite matrix (a) and its further transformation to Fourier image (b) [2]. Comprehensive experimental studies on ODS steels with atomic resolution performed recently at IMF-1, FZK, Karlsruhe show stability of pure Y_2O_3 -ODS and yttria nanoparticles.

Atomistic simulation of the precipitation kinetics is necessary for understanding of basic mechanisms and for improvement and optimization of technology of ODS steel

production. A simplified model of ODS formation would include impurity atoms (Y and O) dissolved in the steel matrix, represented by γ -Fe. We propose theoretical approach for atomistic simulations of this process in two steps. As the first step, extensive *ab initio* calculations of simple yttrium and oxygen complexes in Fe lattice containing also point iron vacancies are performed. The results of these calculations are used then in the kinetic Monte Carlo (MC) simulations of Y_2O_3 particle growth. The simplest MC model includes diffusion of Y and Fe atoms through a vacancy mechanism. We studied an interstitial oxygen atom in both. A barrier of O migration between the octahedral and tetrahedral interstitials of Fe-lattice (where oxygen atom can be located) is expected to be lower than that of self-diffusion and vacancy-assistant yttrium diffusion. Therefore, slow diffusion of large Y atoms is a *rate-determining process* in oxide particle formation. In this model, we assume that oxygen can quickly accommodate to the slow component motion.

3.4.2.3 Results

The first step of multi-scale modelling of ODS particle formation in steel performed in collaboration with *IMF I, Karlsruhe*, has included large-scale VASP calculations on *fcc* lattice of γ -Fe with further inclusion of O and Y impurities and formation of Fe vacancies (Figure 3.4.2.3.1). Together with calculated pair-wise interactions (Fe-O, Fe-vacancy, Fe-Y, O-O vacancy-O, O-Y vacancy-vacancy, vacancy-Y and Y-Y) as well as energy barriers for diffusion of impurities and vacancies supply us with the necessary parameters for further kinetic simulations. VASP calculations have been performed for large Fe supercells (at least for $4 \times 4 \times 4$ extension using full geometry optimization). We have developed the methodology for these calculations, choosing proper sets of computational parameters as well as electronic and magnetic states of systems. The Perdew-Wang-91 GGA (Generalized Gradient Approximation) non-local exchange-correlation functional and the scalar relativistic PAW (Projected Augmented Wave) pseudopotentials have been used. The pseudopotentials describe the core electrons of Fe ($4s^1 3d^7$ external shell), O ($2s^2 2p^4$) and Y ($4s^2 4p^6 5s^1 4d^2$) atoms with 8, 6 and 11 external electrons, respectively. The Monkhorst-Pack scheme for $12 \times 12 \times 12$ *k*-point mesh in the Brillouin zone was used. At hipping temperature of $\sim 1100^\circ\text{C}$ γ -Fe has been assumed to be non-magnetic.

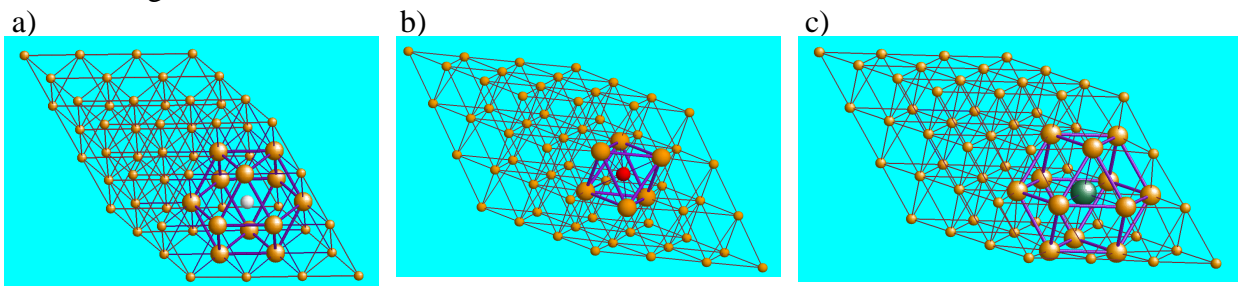


Figure 3.4.2.3.1 $4 \times 4 \times 4$ supercell of face-centered-cubic (*Fm3m*) structure of γ -Fe containing a single iron vacancy (a), oxygen atom located at the centre of octahedron interstitial (b) and yttrium atom incorporated in position of Fe vacancy (c). These structures exhibit the equilibrium geometry obtained in our calculations.

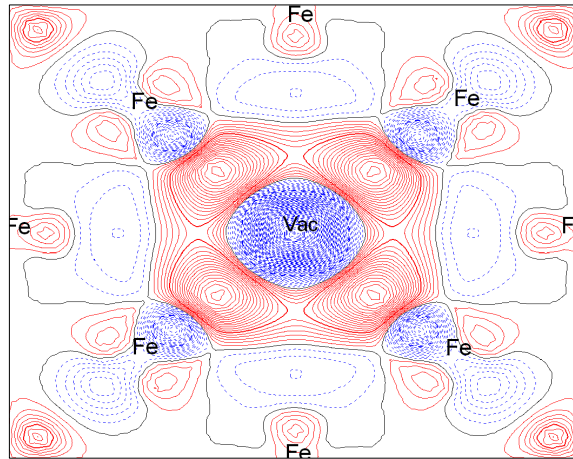
We have calculated key parameters of the atomic and electronic structure for all configurations described above: lattice parameter and bulk modulus, densities of states (DOS) and band structure, equilibrium geometry of defective structures around vacancies and impurities re-distributions of electronic and spin densities in *fcc*-Fe under

influence of vacancies and impurities. Presence of a single iron vacancy noticeably re-distributes the electronic density in iron matrix (Figure 3.4.2.3.2. a). We also estimate migration barriers of Fe vacancy, O and Y impurity atoms inside the γ -Fe lattice. The vacancy formation energy for $4\times 4\times 4$ supercell has been found to be 2.95 eV with 0.75% inward relaxation.

The energy gain due to insertion of O atom at the centre of octahedron formed by the nearest six Fe atoms has been found to be 3.21 eV per $4\times 4\times 4$ supercell whereas relaxation energy is 2.67 eV which is necessary for expansion of the first coordination sphere around impurity atom by ~ 9 percent. It was found that O impurities possess excessive electronic charge -1.3-1.4 e (Figure 3.4.2.3.2. b). Y impurity atom can only substitute Fe atom in its vacancy (in the centre of cuboctahedron formed by the nearest twelve Fe atoms) serving as a donor of electronic density ($\sim 1 e$). As a result, the electronic density in iron matrix is markedly re-distributed (Figure 3.4.2.3.2. a). The energy gain due to insertion of Y atom into γ -Fe lattice can be considered as 0.71 eV (substantially smaller than after insertion of oxygen impurity) with relaxation energy 1.40 eV and 7% expansion of the first coordination sphere (Fig. 3.4.2.3.2. c).

For optimization of O atom diffusion path, we have considered the centre of triangle between the nearest tetrahedron and octahedron of γ -Fe lattice as a saddle point of the corresponding trajectory. A barrier of O migration between them has been found to be 1.62 eV, very close to experimental result published in [8]. To determine the optimal distance between the two Y impurity atoms, we have increased the Y-Y distance inside the $4\times 4\times 6$ supercell. According to our estimate *via* construction of the potential curve depending on Y-Y distance the minimum has been formally found to be between the second and third Y next-neighbour site which is not stable for location of O impurity atom while repelling occurs at 1 NN distance. Preliminary kinetic Monte-Carlo simulations performed synchronously with DFT calculations confirm a possibility of yttrium clustering even without presence of oxygen. Further steps of theoretical simulations should include small clusters containing Fe vacancies as well as O and Y impurity atoms.

a)



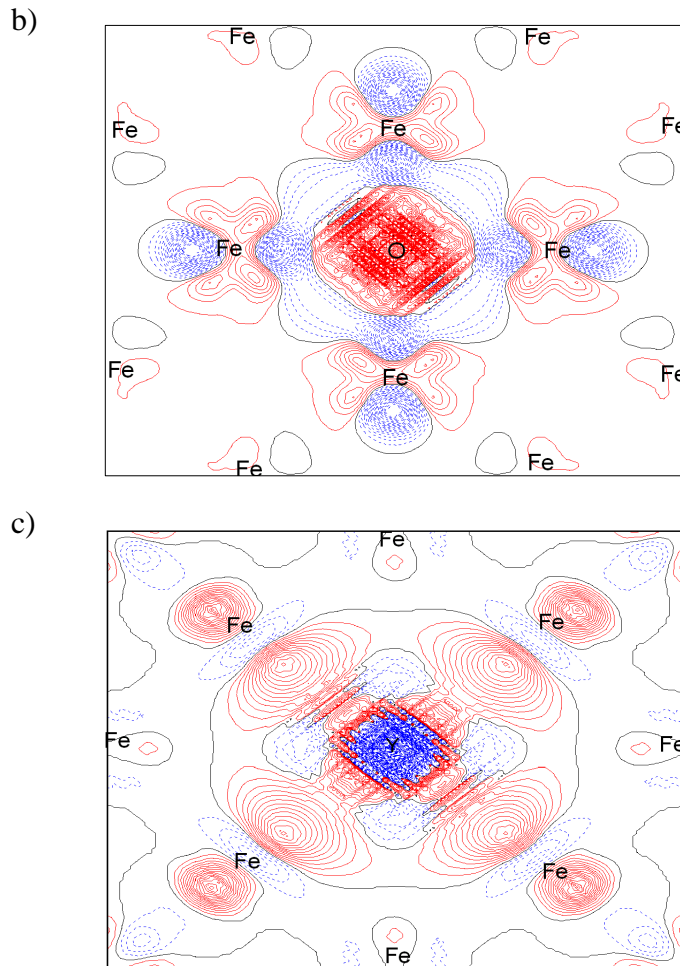


Figure 3.4.2.3.2. The calculated (110) cross sections of the difference electron density maps $\Delta\rho(r)$ for γ -Fe $4\times 4\times 4$ supercell containing a single iron vacancy (a), oxygen atom located at the centre of octahedron interstitial (b) and yttrium atom incorporated in position of Fe vacancy (c) – see Fig.3.4.4.4 for better understanding of the corresponding models. $\Delta\rho(r)$ is defined as the total density in the optimized structures of defective γ -Fe bulk (a), γ -Fe+O (b) and γ -Fe+Y (c) minus the sum of electron densities of Fe, O and Y atoms positioned in the centres of defective fcc lattices and relaxed lattices without them. Dash-dot (black) isolines correspond to the zero level. Dashed (blue) isolines stand for a decrease in $\Delta\rho(r)$ and solid (red) lines for an increase. Chemical symbols of sectioned atoms are shown inside the plots.

3.4.2.4 Conclusions

1. The first step of multiscale modelling of ODS particle formation in steel has included large scale VASP calculations on fcc lattice of γ -Fe with further inclusion of Y and O impurities and formation of Fe vacancies. Together with calculated pair-wise interactions (Fe-vacancy, Fe-Y, Fe-O, vacancy-vacancy, vacancy-Y, vacancy-O, Y-Y, Y-O and O-O) energy barriers for diffusion of impurities and vacancies supply us with the necessary parameters for further kinetic simulations.

2. Our preliminary results show that dissolved yttrium atoms tend to precipitate in a form of particles coherent with the iron matrix. This suggests that the final orientation of oxide particles and surrounding matrix might depend on the matrix phase transformation.

3. Further calculations should be oriented on more complicated configurations of Fe vacancies, Y substitutes and O impurities, which include not only their pairs but triples and quartets as well.

4. EFDA FUSION TECHNOLOGY PROGRAMME

The fusion technology work has been performed at the Institute of Chemical Physics, University of Latvia in very close co-operation with EURATOM- UKAEA Culham and EURATOM- FZK, Germany as well as at the Institute of Solid State Physics, University of Latvia in co-operation with EURATOM IPP, Garching.

Institute: **ICP UL – Institute of Chemical Physics, University of Latvia**

Research scientists: Dr. Gunta Kizane
Bsc. Elina Kolodinska
Bsc. Ingars Reinholds
Dr. Juris Tiliks
Dr. Vija Tilika
Dr. Aigars Vitins

4.1. Magnetic field effect on technologies for detritiation of beryllium materials

Principal investigator G. Kizane

4.1.1. Introduction

Tritium retention in the volume and subsurface layers of Be materials in both JET and ITER is an undesirable phenomenon. Present in-situ detritiation technologies are based on increase of temperature in Be surface layer, which stimulates tritium diffusion in Be crystal lattice. Though tritium in metal Be forms gas dynamic solution, where tritium is in an atomic form, nevertheless, T_2 may form at a high tritium concentration. The release of molecular tritium T_2 is impeded under the action of the energy carriers used in the present detritiation technologies. In order to take out the molecular tritium T_2 localised in Be on grain boundaries, dislocations, micropores, etc., dissociation of T_2 into T^0 is necessary. The minimum energy that is necessary for the dissociation is 4-5 eV per molecule, which is difficult to be achieved in inner layers of Be only by action of light quanta. Even after dissociation of T_2 into a pair of radicals T^0 , there is a high probability of their further recombination, as the pair of radicals will form with correlated spins, i.e. in a singlet state. That will decrease the amount of T^0 and will delay the tritium release from Be. In the year 2005, investigating the tritium release from the irradiated Be pebbles, a novel synergetic effect was observed in our laboratory. The synergetic effect is a considerable increase in the tritium release under the simultaneous action of high temperature, ionising radiation and intense magnetic field. For instance, annealing the Be pebbles at a constant temperature 1123 K for 2 h under the simultaneous action of the magnetic field of 1.7 T and the fast electron radiation ($P=14 \text{ MGy}\cdot\text{h}^{-1}$), tritium was released by 80% more than that was released under the only action of temperature 1123 K for 2 h. The effect might be explained by the spin transformation in a pair of radicals T^0 caused by the magnetic field. The spin transformation reduces the probability of the following recombination. It is anticipated that the same process will take place in subsurface layers of Be materials, particularly in

the case of high tritium concentrations, when T₂ molecules have formed in the metal. Effects of magnetic field might also be observed in the application of detritiation technologies (laser radiation, plasma treatment, etc.).

The main objective of the project for the year 2007 consisted of the following items:

- to investigate effects of separate and simultaneous electron radiation and magnetic field (MF) on tritium release from the real JET irradiated Be tiles in a gas flow mode;
- to evaluate appropriateness of the combined treatment (simultaneous temperature, MF and radiation) for technology of detritiation of Be tiles

4.1.2. Organizational arrangements

A new project proposal “Determination of tritium and analysis of carbon-based plasma-facing components before and after their detritiation with different methods” has been prepared by the Laboratory of Radiation Chemistry of Solids of the University of Latvia for the EFDA JET Technology Workprogramme 2008 and accepted as Task JW8-FT-1.12.

4.1.3. Methodical undertakings

Setups and methods for determination of chemical forms of localized tritium and their distribution were optimized. A radiation thermal magnetic rig for investigation of tritium release under simultaneous action of temperature, radiation and magnetic field was improved by introducing the following changes:

- a new heater has been made;
- a new quartz tube for samples cut from the Be tiles irradiated in JET has been made for continuous measuring of tritium release at annealing in a gas flow mode;
- a new thermocouple of type S is used. A thermocouple of type S is compatible with the temperature control unit of the rig.

The radiation thermal magnetic rig was tested and adjusted for investigations of tritium release from samples cut from irradiated Be tiles under separate and simultaneous action of temperature, radiation and magnetic field.

4.1.4. Experimental techniques and methods

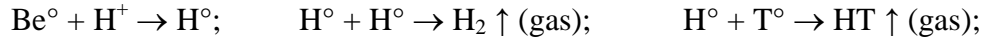
4.1.4.1. Preparation of Be samples

Irradiated beryllium tiles (size 25×8×3 cm, mass 970 g) manufactured by hot isostatic pressing were investigated in this study. The irradiated Be tiles had been used in the upper belt limiter in the vacuum vessel of the Joint European Torus (JET, Culham, UK) in the D+D and D+T experimental campaigns in 1989-1992. Average tritium activity in these Be tiles was 1130 Bq·g⁻¹. The two irradiated Be tiles investigated were denoted as tiles “A” and “B”. Samples (discs, plates) for dissolution and thermo-annealing experiments from the operating surface of the Be tiles were prepared by drilling with core drills or cutting with hard-facing or diamond milling cutters. Samples having a defined surface area about 0.5 cm² and thickness of 2 mm were cut from separate “teeth” of the operating surface of a Be tile. The Be samples were used for analysis of chemical forms of localized tritium and their distribution along a depth, and for investigations of tritium release at annealing. Mechanical treatment of Be tiles was performed both in ambient air atmosphere and under water layer. Location of Be

samples under water even for a long time (up to 24 h) does not change amount and chemical forms of localized tritium.

4.1.4.2. Lyomethod of tritium analysis for Be samples

In order to determine tritium distribution in a Be tile along a depth from the operating surface and chemical forms of tritium (T_2 , T^0 , T^+), two adjacent samples were cut from the surface of a Be tile and dissolved in pure 2 mol/L H_2SO_4 and in a solution of 2 mol/L H_2SO_4 + 0.5-1 mol/L $Na_2Cr_2O_7$ in a special setup. The following chemical reactions take place at dissolution of a Be sample containing the different chemical forms of tritium (T_2 , T^0 , T^+) in pure 2 mol/L H_2SO_4 :



Be dissolving in acid forms hydrogen – 1 molecule of H_2 corresponding to 1 Be atom. The rate of hydrogen evolution, which characterizes the rate of dissolution of a Be layer, was determined with a catarometer. The T_2 and T^0 localized in a Be layer transfers as T_2+HT into a gas phase, its rate of release was measured continuously with a gas flow-through proportional detector DDH 32 of the operating volume 300 cm^3 built in a meter TEM-2100A. The tritium activity released into a gas phase at dissolution in the pure acid, $A_{T_gas_acid}$, is a sum of the activities of T_2 and T^0 : $A_{T_gas_acid} = A_{T_2} + A_{T^0}$. T^+ localized in a Be layer remains in the solution. After the dissolution of a Be layer of defined thickness (400-500 μm), the tritium activity in the solution, $A_{T_sol_acid}$, was measured with a liquid scintillation method: $A_{T_sol_acid} = A_{T^+}$, where A_{T^+} – the activity of T^+ in the beryllium dissolved.

In order to determine the chemical forms of tritium T_2 and T^0 separately, it is necessary to perform 2 dissolution experiments with identical Be samples – only in acid and in acid with a scavenger of H° (T^0) (0.5-1 mol/L $Na_2Cr_2O_7$), which decreases H° (T^0) by 90%:



Then the activity of the tritium released into a gas phase and retained in the solution are the respective sums: $A_{T_gas_Cr(VI)} = A_{T_2} + x \cdot A_{T^0}$ and $A_{T_sol_Cr(VI)} = A_{T^+} + (1-x) \cdot A_{T^0}$, where $x = n_{H_2} / n_{Be}$ (x was found to be 0.1); n_{H_2} – the molar amount of the hydrogen evolved at the dissolution; n_{Be} – the molar amount of the beryllium dissolved at the dissolution. The contents of T_2 , T^0 , T^+ ($Bq \cdot cm^{-2}$ or $Bq \cdot g^{-1}$) in a sample were determined separately from the corresponding differences in the activities.

4.1.4.3 Technique of annealing of Be samples

Annealing of Be samples was performed in a continuous flow of the purge gas He + 0.1 % H_2 of the rate 14.3 ± 0.5 L/h without and in MF of 1.7 T and/or 5 MeV fast-electron radiation at the dose rate $P=14$ $MGy \cdot h^{-1}$ in a special rig. The tritium released was measured continuously with a meter TEM 2100A with a detector DDH 32. The sample temperature was increased linearly with time at the rate 5 K/min from a room temperature to an end temperature 773 ± 5 K, which was kept constant within ± 5 K for 30 min. Then the heater was switched off, and the sample was left to cool in a flow of the purge gas. The annealing temperature of 773 K for investigations of additional effects of radiation and MF on tritium desorption was selected on the basis of curves of

tritium release in a continuous gas flow, annealing a Be sample at a constant rate of 5 K/min from a room temperature to 1126 K so that only a part of the total tritium is released at 773 K for 30 min. The radioactivity of tritium released was calculated as Bq·cm⁻² to 1 cm² of the plasma-exposed surface area.

4.1.5. Results

4.1.5.1. Chemical forms of tritium localized in surface layers of Be tiles

Using the lyomethod, abundance ratios of chemical forms of sorbet tritium were determined in the irradiated Be tile “A” and compared in Table 4.1.5.1.1. with those of the irradiated Be tile “B”. It should be noted that the amount of the retained tritium is different in various places of the plasma-facing surface of the Be tiles. The total tritium activity (Bq·cm⁻²) calculated for 1 cm² of the plasma-exposed surface area of different samples of the plasma-facing surface of tile “A” was found in the range 10-60 kBq·cm⁻², but that of tile “B” was 2.4-4.8 kBq·cm⁻². The non-homogeneous distribution of tritium on the plasma-facing surface limited the accuracy of the determination of the abundance ratios of chemical forms of tritium as the identity of the two samples is essential for this determination. By a factor of ≥ 4 lower tritium concentration was found for the lateral surface of Be tile “B” and for the surface facing a gap between teeth. A little T⁺ (0.45 kBq·cm⁻²) was found in surface layers beneath the plasma-melted surfaces.

Table 4.1.5.1.1. The total tritium activity, A_T, and abundance percentages of chemical forms of tritium localized in the irradiated Be tiles

Tile	Surface	A _T , kBq·cm ⁻²	T ₂	T ⁰	T ⁺
“A”	Plasma-facing	31.7	44%	42%	14%
“B”	Plasma-facing	4.8	73%	16%	11%
“B”	Lateral	0.6	60%	25%	15%
“B”	Gap between teeth	0.3	47%	20%	33%
“B”	Plasma-melted	0.45	-	-	100%

4.1.5.2. Tritium release at annealing

Curves of the fractional tritium release at annealing of samples of Be tile “A” are shown in Fig. 4.1.5.2.1. The fractional tritium release was calculated as the ratio of the activity of tritium released into the gas phase at the annealing to the initial total activity of tritium localized in the sample. For the experiments TM and TRM, the magnetic field was switched on before the start of the temperature program and switched off after the end of the temperature program, after cooling the samples below 470 K. For the experiments TR and TRM, the electron radiation was switched on in a few minutes after the start of the temperature program and switched off after the end of the temperature program, after cooling the samples below 470 K. The start of electron radiation is evident as a steep increase in the temperature above the programmed rate of 5 K/min in the time range of 35-50 min in the temperature curves in Fig. 4.1.5.2.1. The efficiency of detritiation of samples of a Be tile under the given conditions can be arranged in the following sequence: T<TM<<TR<TRM. The initial total activity of tritium (kBq·cm⁻²) for these samples was determined after their dissolution: T – 24.6, TM – 24.9, TR – 16.5, TRM – 23.5. The degrees of detritiation obtained in these experiments are compared in Fig. 4.1.5.2.2. with those obtained in previous ampoule experiments at

constant temperatures with samples of another similar D-T plasma-exposed Be tile “B” from JET and the Be pebbles irradiated in the BERYLLIUM experiment in 1994.

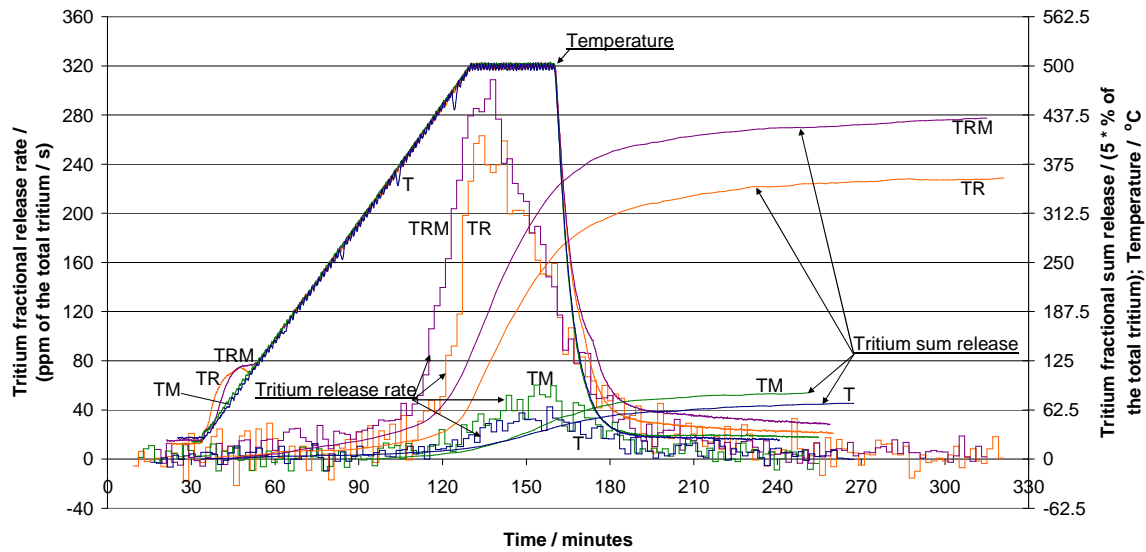


Figure 4.1.5.2.1 Tritium fractional release at annealing of samples of Be tile “A” in a continuous flow of He + 0.1 % H₂. Curve labels denote: T – action of the given temperature; M – magnetic field of 1.7 T; R – 5 MeV fast-electron radiation of 14 MGy·h⁻¹.

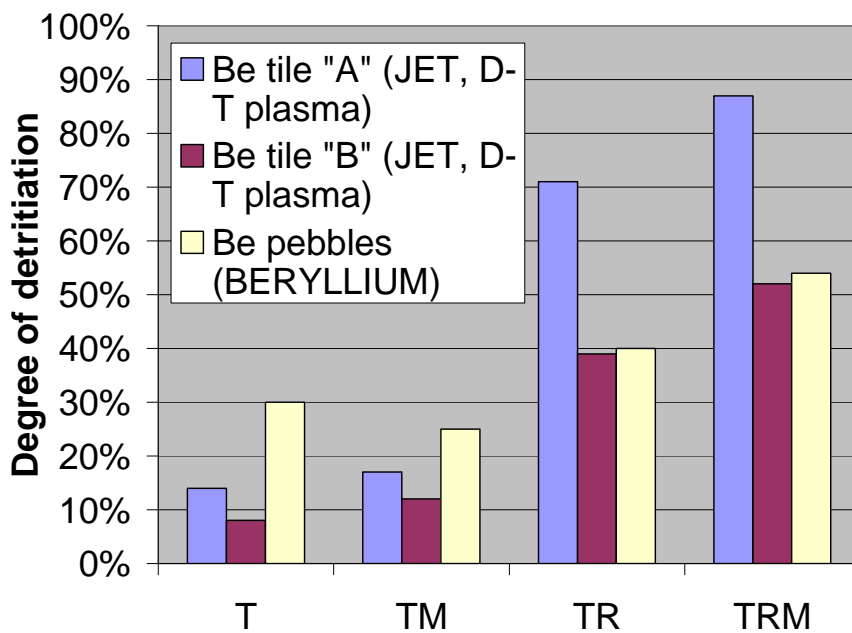


Figure 4.1.5.2.2 Comparison of degrees of detritiation of JET Be tiles and BERYLLIUM pebbles under the following conditions of annealing: Be tile “A” – ramp of 5 K/min to 773 K and at 773 K for 0.5 h in a continuous flow of He + 0.1 % H₂; Be tile “B” – a constant temperature 773 K for 0.5 h in an ampoule; Be pebbles (BERYLLIUM) – a constant temperature 1123 K for 2 h in an ampoule. Category axis labels denote: T – action of the given temperature; M – magnetic field of 1.7 T; R – fast-electron radiation of 14 MGy·h⁻¹

4.1.6 Discussion

The results obtained show that Be tile “A” has a higher tritium activity by a factor of about 5 of the plasma-exposed surface and a greater abundance of atomic tritium T^0 by a factor of about 2.5 than Be tile “B”. That means that different Be tiles of the upper belt limiter of JET have considerably different tritium activities of the plasma-facing surface and abundance ratios of chemical forms of tritium.

Higher values of the degree of detritiation of tile “A” than that of tile “B” may be due to the different experimental conditions and a greater abundance ratio of faster diffusing atomic tritium T^0 in tile “A” than in tile “B”.

The facilitating effect of fast-electron radiation on the tritium release can be related to radiolysis of tritium localized in the molecular T_2 form into faster diffusing atomic T^0 particles. Fast-electron radiation has a considerably more facilitating effect on the detritiation of the Be tiles than that of the irradiated Be pebbles (Fig. 4.1.5.2.2.). Though the Be pebbles have a greater abundance ratio of molecular tritium T_2 85%, the higher effect of radiation in the case of tiles may be explained by the fact that unlike the pebbles, most of the tritium in the tiles is localized in a subsurface layer of 60 μm . Similarly to the tritium release of the irradiated Be pebbles, the synergetic effect of simultaneous radiation and MF on the tritium release of the Be tiles was observed (Fig. 4.1.5.2.2.). The synergetic effect might be explained by the fact that MF causes the spin transformation in pairs of radicals $T^0 \cdots T^0$ and thus reduces the probability of the following recombination and increases the concentration of T^0 in a Be matrix.

4.1.7 Conclusions

Abundances of chemical forms of tritium in a plasma-facing surface layer of Be tile “A” was evaluated: T_2 – 44 %, T^0 – 42 %, T^+ – 14 %. That differs from the abundances determined previously for tile “B”: T_2 – 69-72 %, T^0 – 18-20 %, T^+ – 9-11 %. Fast-electron radiation considerably increases the fractional tritium release at annealing by a factor of approx. 5. Magnetic field increases the fractional tritium release at annealing both without and under electron radiation by approx. 25 %.

4.2 Assessment of the effects of magnetic field, radiation and temperature on the tritium release from beryllium pebbles. Identification of chemical forms of tritium accumulated in the irradiated beryllium pebbles.

4.2.1 Introduction

The project objective for the year 2007 was to test the stimulating effect of the simultaneous action of magnetic field (MF), temperature and ionizing radiation on the tritium release from the Be pebbles irradiated in the EXOTIC 8-3/13 experiment. The stimulating effect was found previously investigating tritium release at annealing the Be pebbles irradiated in the BERYLLIUM experiment. The tritium accumulation in Be pebbles is an important issue of the blanket technology. That may be related to both the mechanical damages of HCPB as a result of swelling and an increase in the environmental hazard in the case of accidental tritium release. Recovery of tritium from the Be pebbles could replenish the tritium used as a fuel in the deuterium-tritium fusion reaction. Present methods of investigation of Be pebbles under the ITER and DEMO relevant conditions (irradiation with a flux of fast neutrons in the fission High Flux Reactor (HFR)) do not enable investigations of the effect of MF of the real intensity on the tritium accumulation. Similarly, no MF effect is modelled in the present code for prediction of the tritium release (the ANFIBE code). According to the version ANFIBE

0, in a range of operating temperatures 715-974 K, about 80% of the tritium will be retained in Be pebbles. The new version ANFIBE 1 predicts a less amount of the retained tritium, however also this version takes no account of possible MF and radiation effect. In order to investigate this effect, annealing of the EXOTIC 8-3/13 irradiated Be pebbles at different constant temperatures without and in MF and under ionizing radiation was envisaged for the year 2007. The reason for such investigations of the EXOTIC 8-3/13 Be pebbles is determined by the fact that these pebbles differ from the BERYLLIUM pebbles in respect of their manufacturing method, their size, their impurity content, their irradiation conditions (time, neutron fluence, irradiation temperature), their ^4He and ^3H content.

4.2.2. Organizational arrangements

1. Samples of the Be pebbles irradiated in the EXOTIC 8-3/13 experiment were received from FZK in January 2007.

2. A new tritium measuring system TEM-2102A has been purchased and set up for measuring of radioactivity of gases in a gas flow mode on a radiation thermal magnetic rig at Salaspils, Latvia.

3. Organizational arrangements for transportation of the Be pebbles irradiated in the pebble bed assembly (PBA) experiment from Petten, the Netherlands, to Riga, Latvia, have been made.

4. A "Cole-Parmer" set of a 150-mm flowmeter KH-03295-10 with a high-resolution valve, a "Precisa" semi-micro balance XR 125SM of the 320XR series and an antivibration table for the balance have been purchased to improve the work place at the radiation thermal magnetic rig at Salaspils, Latvia.

4.2.3. Methodical undertakings

Setups and methods for determination of chemical forms of localized tritium and their distribution were optimized.

The radiation thermal magnetic rig was tested and adjusted for investigations of tritium release from irradiated Be pebbles under separate and simultaneous action of temperature, radiation and magnetic field.

4.2.4. Experimental methods and techniques

4.2.4.1 Samples investigated

The beryllium pebbles irradiated in the EXOTIC-8-3/13 experiment were investigated in this study. These pebbles of a diameter 0.1-0.2 mm have been manufactured by spraying molten beryllium in an inert atmosphere (inert gas atomization process, IGA) at Brush Wellman Inc. Their grain size is 40 to 200 μm . The main impurities are 3400 ppm BeO, 100 ppm Mg. The pebbles were irradiated for 449.8 days in the High Flux Reactor (HFR) at Petten, the Netherlands, at temperatures 800-900 K with a neutron fluence of $2.7 \cdot 10^{25} \text{ m}^{-2}$ ($E > 0.1 \text{ MeV}$) of a fast fission spectrum. The ^4He content of 285 appm and the ^3H content of 1.16 appm (i.e. 138 MBq/g) at the end of the irradiation in the year 2000 were calculated on the basis of the irradiation history.

4.2.4.2 Lyomethod of tritium analysis

In order to determine the total tritium activity and abundance ratios of chemical forms of tritium (T_2 , T^0 , T^+) in irradiated beryllium pebbles, two weighed amounts of the pebbles were dissolved in pure 2 mol/L H_2SO_4 and in the solution 2 mol/L H_2SO_4 + 0.5-

1 mol/L $\text{Na}_2\text{Cr}_2\text{O}_7$ in a special setup. Be dissolving in pure acid forms hydrogen – 1 molecule of H_2 corresponds to 1 Be atom. The rate of hydrogen evolution was measured with a catarometer. The T_2 and T^0 localized in a Be layer transfer as $\text{T}_2 + \text{HT}$ into a gas phase, the rate of release of that was measured continuously with a gas flow-through proportional meter TEM 2100A with a detector DDH 32 of the operating volume 300 cm^3 . The tritium activity released into a gas phase at the dissolution in the pure acid, $A_{\text{T}_{\text{gas_acid}}}$, is a sum of the activities of T_2 and T^0 : $A_{\text{T}_{\text{gas_acid}}} = A_{\text{T}_2} + A_{\text{T}^0}$. T^+ localized in a Be layer remains in the solution. After the Be pebbles had completely dissolved, the tritium activity in the solution, $A_{\text{T}_{\text{sol_acid}}}$, was measured with liquid scintillation method: $A_{\text{T}_{\text{sol_acid}}} = A_{\text{T}^+}$, where A_{T^+} – the activity of T^+ in the sample dissolved. In the second dissolution experiment the scavenger of H^0 (T^0) – 0.5-1 mol/L $\text{Na}_2\text{Cr}_2\text{O}_7$ decreases H^0 (T^0) by 90%: $\text{H}^0 + \text{Cr}_2\text{O}_7^{2-} \rightarrow \text{H}^+$ (solution) + Cr^{3+} . Then the activity of the tritium released into a gas phase and retained in the solution are the respective sums: $A_{\text{T}_{\text{gas_Cr(VI)}}} = A_{\text{T}_2} + x A_{\text{T}^0}$ and $A_{\text{T}_{\text{sol_Cr(VI)}}} = A_{\text{T}^+} + (1-x) A_{\text{T}^0}$, where $x = n_{\text{H}_2} / n_{\text{Be}}$ (x was found to be 0.1); n_{H_2} – the molar amount of the hydrogen evolved at the dissolution; n_{Be} – the molar amount of the beryllium dissolved. The contents of T^0 , T_2 , T^+ ($\text{Bq} \cdot \text{g}^{-1}$) in a sample were determined separately from thermal magnetic rig for investigation of tritium release under simultaneous action of temperature, radiation and magnetic field was improved by the introduction of the following changes:

- a new heater has been made;
- a new quartz tube for the fine Be pebbles irradiated in the EXOTIC 8-3/13 experiment has been made for continuous measuring of tritium release at annealing in a gas flow mode;
- a new thermocouple of type S is used. A thermocouple of type S is compatible with the temperature control unit of the rig. Corresponding differences in the activities: $A_{\text{T}^0} = (A_{\text{T}_{\text{gas_acid}}} - A_{\text{T}_{\text{gas_Cr(VI)}}}) / (1-x)$; $A_{\text{T}_2} = A_{\text{T}_{\text{gas_acid}}} - A_{\text{T}^0}$; $A_{\text{T}^+} = A_{\text{T}_{\text{sol_acid}}}$.

4.2.4.3 Tritium release at annealing

Annealing of Be samples was performed in a continuous flow of the purge gas He + 0.1 % H_2 of the rate $14.3 \pm 0.5 \text{ L/h}$ without and in MF of 1.7 T and/or 5 MeV fast-electron radiation of the dose rate $P=14 \text{ MGy} \cdot \text{h}^{-1}$ in a special rig or in a continuous flow of the purge gas argon of the rate $15 \pm 1 \text{ L/h}$ in another setup where MF up to 2.35 T can be applied without the fast-electron radiation. The tritium released was measured continuously with a meter TEM 2100A with a detector DDH 32. In the experiments, the sample temperature was increased linearly with time at the rate 5 K/min from a room temperature to the end temperature selected from the range 773 - 1123 K, which was kept constant within $\pm 5 \text{ K}$ for 47 to 240 min. Then the heater was switched off, and the sample was left to cool in a flow of the purge gas. The annealing temperature of 940 K for investigations of additional effects of radiation and MF on tritium desorption was selected on the basis of curves of tritium release in a continuous gas flow annealing a Be sample at a constant rate of 5 K/min from a room temperature to 1123 K so that only a part of the total tritium is released at 940 K for 47 min. The radioactivity of tritium released was calculated as $\text{Bq} \cdot \text{g}^{-1}$ to 1 g of the sample of Be pebbles.

4.2.5 Results and discussion

4.2.5.1 Chemical forms of tritium

Using the lyomethod, abundance ratios of chemical forms of tritium localized in the EXOTIC-8-3/13 irradiated Be pebbles were determined. These values are compared in Table 4.2.5.1.1. with other values determined for the BERYLLIUM irradiated Be

pebbles and subsurface layers of the plasma facing surface of the JET D-T plasma exposed upper belt limiter Be tiles.

Table 4.2.5.1.1. The total tritium activity, A_T , and abundance percentages of chemical forms of tritium localized in irradiated beryllium samples

Beryllium sample	A_T	T_2	T^0	T^+
EXOTIC-8-3/13 pebbles	4-18 MBq/g	65%	23%	12%
BERYLLIUM pebbles	0.6-1.5 GBq/g	85%	10%	5%
JET tile "A"	31.7 kBq/cm ²	44%	42%	14%
JET tile "B"	4.8 kBq/cm ²	73%	16%	11%

It should be noted that the EXOTIC-8-3/13 Be pebbles were found to be inhomogeneous with respect to the total tritium activity, A_T , which was found in the range 4-18 MBq/g. This inhomogeneity of the sample limited the accuracy of the determination of the abundance ratios of chemical forms of tritium as the identity of the two samples is essential for this determination. We can see that the most part of tritium in the EXOTIC-8-3/13 Be pebbles, similarly to the BERYLLIUM pebbles and the JET tile "B", is localized as molecular tritium T_2 , but the abundance ratios of T^0 and T^+ in the EXOTIC-8-3/13 Be pebbles are about by a factor of two greater than those in the BERYLLIUM pebbles.

4.2.5.2 Tritium release at annealing

In order to investigate possible effect of MF on tritium release from the Be pebbles irradiated in the EXOTIC-8/13 experiment, they were annealed at a constant rate of temperature increase to 991 and 1123 K and then at a constant temperature for 4 h in a flow of argon of 15 L/h, the curves of tritium release are given in Fig. 4.2.5.2.1. At heating, at about 900-940 K, the slope of the curves of the tritium release rate increases, which can be explained that additional channels for the tritium release open. Subsequent dissolution experiments indicated that no tritium remained in the pebbles after annealing at 1123 K for 4 h. Therefore a complete detritiation of the EXOTIC-8/13 Be pebbles was achieved in this treatment. The curves in Fig. 4.2.5.2.1.b testify no appreciable MF effect on the tritium release. On the other hand according to results of the dissolution experiments, a larger fraction of the residual tritium of 13.3% had remained after annealing at 991 K for 4 h in MF of 2.35 T in comparison with 3.4% in the case of annealing without MF (Fig. 4.2.5.2.1.a), which testifies that under the given conditions MF of 2.35 T decreased the fractional tritium release by about 10%.

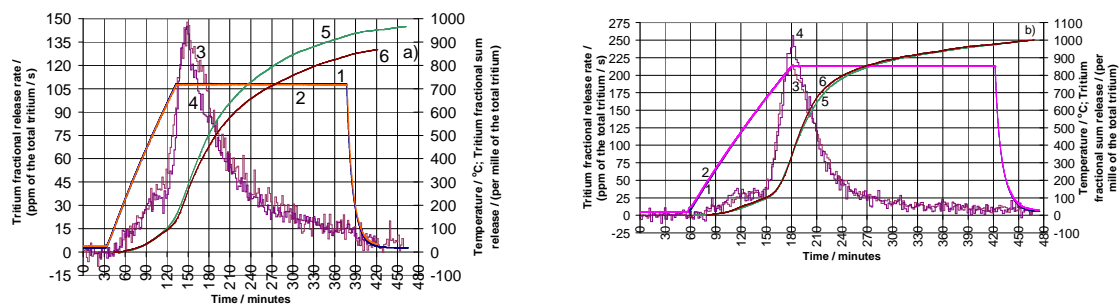


Figure 4.2.5.2.1. Tritium fractional release rate (3, 4) and tritium fractional sum release (5, 6) at annealing of the EXOTIC-8-3/13 Be pebbles at a given temperature (1, 2) – a constant rate of temperature increase and at a constant temperature of 991 K \pm 4

K (a) and $1123\text{ K} \pm 2\text{ K}$ (b) for 4 h without (1, 3, 5) and in MF of 2.35 T (2, 4, 6). The purge gas – argon $15 \pm 1\text{ L/h}$. The tritium fractional sum release has been calculated for the following values of the initial total tritium activity for 1 g of the sample, MBq/g: 7.98 (a, 5); 9.34 (a, 6); 10.69 (b, 5); 11.52 (b, 6)

Experiments in the radiation thermal magnetic rig show that the electron radiation (TR) and the simultaneous electron radiation and magnetic field (TRM) stimulates the tritium release at annealing in comparison with the action of only temperature of 940 K for 47 minutes (Fig. 4.2.5.2.2.). Degrees of detritiation obtained in these experiments are compared in Fig. 4.2.5.2.3. with those obtained in previous experiments with samples of different beryllium articles under different conditions of their annealing. We can see from the experimental results obtained that under similar conditions the detritiation of the EXOTIC Be pebbles proceeded easier than that of the

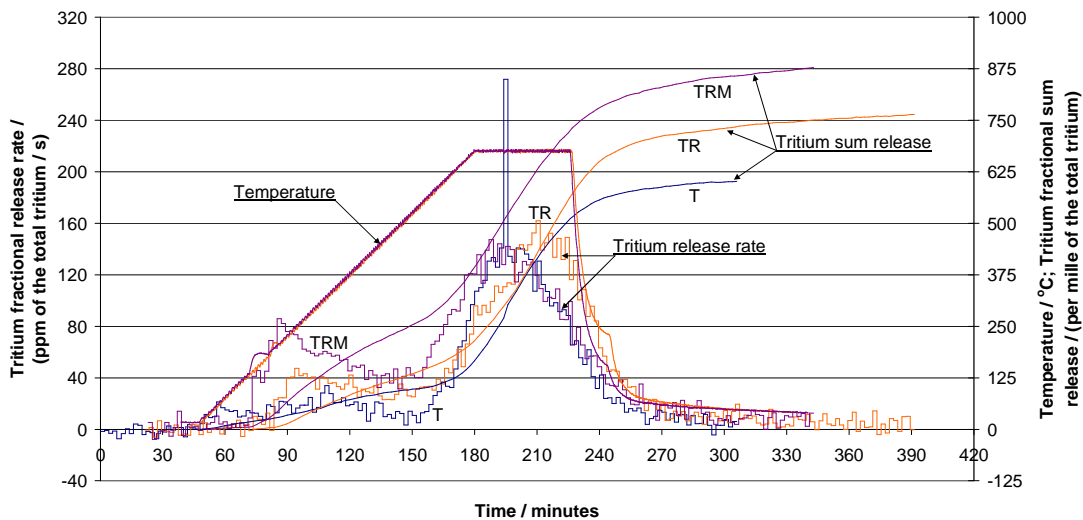


Figure 4.2.5.2.2. Tritium fractional release at annealing of samples of the EXOTIC-8-3/13 Be pebbles in a continuous flow of $14.3 \pm 0.5\text{ L/h}$ of $\text{He} + 0.1\% \text{ H}_2$. Curve labels denote: T – action of the given temperature; M – magnetic field of 1.7 T; R – 5 MeV fast-electron radiation of 14 MGy/h. The tritium fractional sum release has been calculated for the following values of the initial total tritium activity, MBq/g: 6.20 (T); 5.76 (TR); 6.15 (TRM)

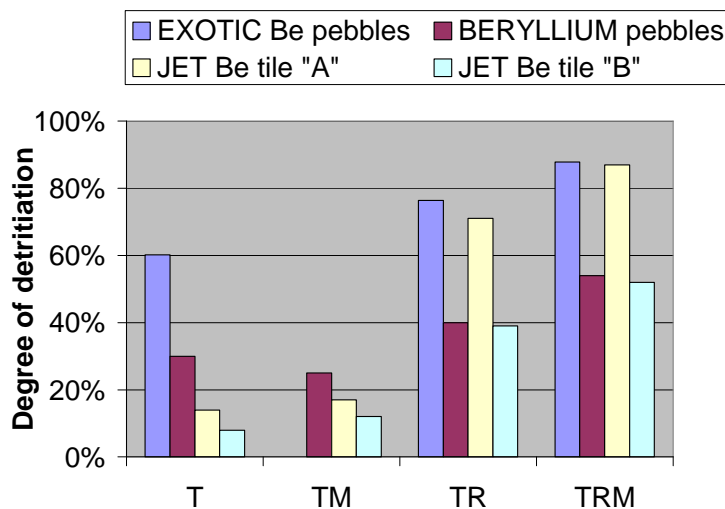


Figure 4.2.5.2.3. Comparison of degrees of detritiation of EXOTIC-8-3/13 and BERYLLIUM pebbles and JET Be tiles under the following conditions of annealing:

EXOTIC Be pebbles – ramp of 5 K/min to 940 K and at 940 K for 47 min in a continuous flow of He + 0.1 % H₂; BERYLLIUM pebbles – a constant temperature 1123 K for 2 h in an ampoule [3]; Be tile “A” – ramp of 5 K/min to 773 K and at 773 K for 0.5 h in a continuous flow of He + 0.1 % H₂ [5]; Be tile “B” – a constant temperature 773 K for 0.5 h in an ampoule [4];. Category axis labels denote: T – action of the given temperature; M – magnetic field of 1.7 T; R – fast-electron radiation of 14 MGy/h

BERYLLIUM pebbles. That can be explained that the EXOTIC pebbles have smaller diameter (\varnothing 0.1-0.2 mm) than the BERYLLIUM pebbles (\varnothing 2 mm) and therefore a larger ratio of free surface to grain boundary surface. A larger abundance ratio of the atomic form T⁰ could also contribute to a higher tritium release of the EXOTIC pebbles. A large degree of detritiation of 60% at 940 K for 47 min of the EXOTIC Be pebbles and a less abundance of the molecular form T₂ possibly could explain that facilitating radiation and MF effects on the degree of detritiation of the EXOTIC Be pebbles are relatively less than those on the detritiation of the BERYLLIUM pebbles.

4.2.6 Conclusions

Abundance ratios of chemical forms of tritium in the beryllium pebbles irradiated in the EXOTIC-8-3/13 experiment were determined: T₂ – 65%, T⁰ – 23%, T⁺ – 12%. A complete detritiation of these pebbles was achieved at 1123 K for 4 h in a continuous flow of argon of 15 ± 1 L/h, MF of 2.35 T had no appreciable effect on the tritium release. At 991K for 4 h, the degree of detritiation was 96.6% without MF, MF of 2.35 T decreased that by about 10% to 86.7%. At 940 K for 47 min, the degree of detritiation was 60%, 5 MeV fast-electron radiation of 14 MGy/h increased that to 76%, but the simultaneous action of the fast-electron radiation and MF of 1.7 T increased that to 88%. Under similar conditions, the detritiation of the EXOTIC-8-3/13 Be pebbles proceeded easier than that of the BERYLLIUM pebbles.

4.3 Development of a prototype of the radiation-hard capacitive bolometer assembly based on ferroelectric material

Principal investigator V. Zauls

4.3.1 Objectives

The work programme is related to the development of radiation resistant diagnostic components and design of pilot model of dielectric bolometer. After initial material studies focussed on processing – microstructure – property relationships of antiferroelectric (AFE) and ferroelectric (FE) sensing film heterostructures for model bolometers optimum choice of materials has been made. The complex characterisation of the fabricated thin film structures included the investigation of various interfaces fabricated during the deposition of heterostructures as well as studies of potential use of antiferroelectric and ferroelectric layers and electrodes in a specific radiation environment. Recent stage of ferroelectric bolometer prototype development brings together former material studies and more detailed prototype engineering aspects including preparation of additional necessary production technologies and optimisation of multilayered structure of selected sensing layer and substrate, buffer layers, bottom / top electrodes and carrier substrate layouts compatible with existing bolometer head assemblies.

4.3.2 Activities to achieve task objectives are listed as follows

- Further work on improvement of required additional *in house* production technologies and characterization techniques to achieve possibility for complete production of ferroelectric bolometer prototype at ISSP LU, such as metal film deposition and possible wiring of contacts to develop more durable electrodes, reliable conductive layers and contact areas compliant with accepted test site requirements.
- Preliminary thermal modelling of proposed new layouts of electrode pattern has been made to ascertain geometry of absorber and electrode contacts of capacitive bolometer prototype structures on non-optimized (thick) substrate for irradiation testing compatible with existing bolometer heads and electrical concepts of detection systems equivalent to Wheatstone bridge arrangements available at test sites. Numerical modelling is used for estimate of the prototype parameters and optimization of absorber shape of the new electrode layout - jointly with IPP Garching and CEA Cadarache.

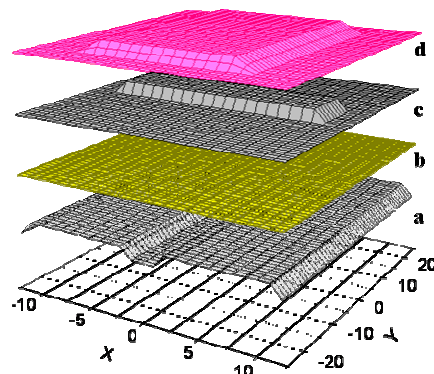


Figure 4.3.2.1 Layers of proposed capacitive bolometric sensor structure: **a** – bottom electrode as two stripes oriented in *y* direction; **b** – active ferroelectric layer; **c** – massive upper electrode (absorber) oriented in *x* direction; **d** – irradiation distribution in input window.

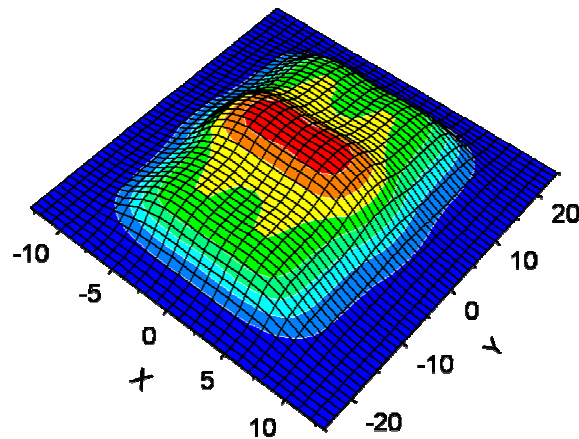


Figure 4.3.2.2 Thermal modelling of temperature distribution demonstrate the main heat deposition area around upper absorber electrode and the heat sink contribution of bottom electrodes to reach thermal balance.

As reported earlier proposed capacitive bolometric sensor structure (Figure 4.3.2.1) consists of substrate (e.g. Si_3N_4 membrane or other) supporting thin ($\sim 1 \mu\text{m}$ thick) parallel bottom Pt electrode gap (a) covered by active ferroelectric material layer (b)

crossed on top by sufficiently thick (~2-4 μm) upper electrode (c) simultaneously acting as absorber. Thus active sensing area is formed by two thin film capacitive spots connected in series, while bottom electrode stripes provide robust wiring outside bolometer window (d) and avoid contact pins to touch active spots.

Numerical simulations of two dimensional heat flows are made according to method proposed for thin membrane and later adapted for gold- Kapton type (*Au-Kap*) bolometer foils. For our example calculation presented here time dependent heat diffusion partial differential equation is solved on a regular grid 27 x 52 grid using forward-time centered-space finite difference scheme and exactly matching with *Au-Kap* numerical model geometry. Our calculation is extended to application in four layer structure to account for thermal parameters and geometric shape of constituents in each layer. Preliminary results of simulated thermal profile are shown in Figure 4.3.2.2 for illustrative purposes. As expected the main heat deposition area around upper absorber electrode is clearly pronounced in temperature distribution and the critical role of bottom electrodes in thermal balance is demonstrated.

4.3.3 Summary

The work programme is related to the development of radiation resistant diagnostic components and design of pilot model of dielectric capacitive bolometer. Recent stage of R&D brings together former material studies and more detailed prototype engineering aspects. Required additional *in house* production technologies and techniques for complete production of ferroelectric bolometer prototype at ISSP (EULA), (for example; such as thick absorber film production, patterned electrode deposition and contact wiring) are still insufficient and should be improved to achieve final task objectives. Additional consulting with external laboratories for engineering knowledge (layer production, packaging) is required for solving production tasks.

Deposition of thick Pt absorber layers has principal importance for production of electrode pattern and reliable contacts of capacitive bolometer prototype structures for irradiation testing compatible with existing bolometer heads and electrical concepts of detection systems equivalent to Wheatstone bridge arrangements available at test sites. Additional numerical modelling has to be continued for estimating the prototype parameters and optimization of active spot size, absorber shape, thickness and electrode layout according to various irradiation scenarios and site requirements.

5. STAFF MOBILITY ACTIONS

5.1 Staff Mobility Visits

Jelena Butikova	worked at IPP Garching from 22 nd October until 20 th November
Elina Kolodinska	worked at Culham Science Centre, Abingdon from 27 th September until 27 th October
Aigars Vitins	took part in the Task Force PWI 2007 General Meeting, CIEMAT, Madrid from 28 th October until 1 st November
Jurijs Zukovskis	worked at Forschungszentrum Karlsruhe from 11 th March until 18 th March and from 28 th September until 13 th October

6. OTHER ACTIVITIES

6.1 Conferences, Workshops and Meetings

Olgerts Dumbrajs participated in the Biennial Workshop Stochasticity in Fusion Plasmas (Jülich, Germany, March 5-7, 2007) and in the 32nd International Conference on Infrared, Millimeter, and Terahertz Waves, Cardiff, UK, September 2 -7, 2007.

Gunta Kizane participated in the 23rd Scientific Conference of the Institute of Solid State Physics of the University of Latvia, dedicated to commemoration of 75 years of Professor Ilmārs Vītols (Riga, Latvia, February 13-15, 2007), in the International Baltic Sea Region Conference “Functional materials and nanotechnologies 2007 (FM&NT-2007)” (Riga, Latvia, April 2-4, 2007), the 8th IEA International Workshop on Beryllium Technology (BeWS-8, Lisbon, Portugal, December 5-7, 2007) and in the 13th International Conference on Fusion Reactor Materials (ICFRM-13, Nice, France, December 10-14, 2007).

Elina Kolodinska participated in the Summer University for Plasma Physics (Greifswald, Germany, September 24-28, 2007) carried out by Max-Planck-Institut für Plasmaphysik at Garching bei München, Germany.

Aigars Vitins participated in the 8th International Symposium on Fusion Nuclear Technology (ISFNT-8, Heidelberg, Germany, September 30 – October 5, 2007).

Jurijs Zukovskis participated in the 13th International Conference on Fusion Reactor Materials ICFRM-13, Nice, France, December, 2007.

6.2 Visits

Olgerts Dumbrajs worked as guest professor at Fukui University, Japan from 1st October until 31st December

6.3 Visitors

Regina Knitter from FZK, Institute for Material Research III visited ICP UL from 28th August until 30th August

7. PUBLICATIONS 2007

7.1 Fusion Physics and Plasma Engineering

7.1.1 Publications in scientific journals

1. R.B. Gomes, H. Fernandes, C. Silva, A. Sarakovskis, T. Pereira, J. Figueiredo, B. Carvalho, A. Soares, C. Varandas, O. Lielausis, A. Klykin, E. Platacis, I. Tale.

"Interaction of a liquid gallium jet with the tokamak ISTTOK edge plasma" Fusion Engineering and Design (submitted) (Available online 24 October 2007).

2. O. Dumbrajs and T. Idehara. "Hysteresis in mode competition in high power 170 GHz gyrotron for ITER" Int. J. Infrared Millimeter Waves (submitted).

3. Z.C. Ioannidis, O. Dumbrajs, and I.G. Tigelis. "Linear and non-linear inserts for genuinely wideband continuous frequency tunable coaxial gyrotron cavities" Int. J. Infrared Millimeter Waves (submitted).

4. Z. C. Ioannidis, G. P. Latsas, I. G. Tigelis, and O. Dumbrajs. "TM Modes in Coaxial Cavities with Inner Surface Corrugations" IEEE Trans. Plasma Sci. (submitted).

5. V. Igochine, O. Dumbrajs, H. Zohm, A. Flaws and ASDEX Upgrade Team. "Stochastic sawtooth reconnection in ASDEX Upgrade." Nuclear Fusion **47**, 23 (2007).

6. O. Dumbrajs, V. Igochine, and H. Zohm, "Diffusion in a stochastic magnetic field in ASDEX Upgrade", Nucl. Fusion (submitted).

7. V. Igochine, O. Dumbrajs, and H. Zohm, "Transition from quasiperiodicity to chaos just before sawtooth crash in the ASDEX Upgrade tokamak" Nucl. Fusion Letters (submitted).

8. V. Igochine, O. Dumbrajs, and H. Zohm, "Transition from quasiperiodicity to chaos just before sawtooth crash in the ASDEX Upgrade tokamak" Nucl. Fusion (submitted).

9. V.N. Kuzovkov and O. Dumbrajs, "Bounded tokamak" Ann. Phys. Craiova Univ. (Romania), **17**, 86 (2007).

10. L. Butikova and I. Tale, "Laser-induced breakdown spectroscopy application for determining impurity content and depth profile in the plasma facing materials" Journal of Nuclear Materials (submitted).

7.1.2 Conference articles

1. V. Igochine, O. Dumbrajs, H. Zohm, A. Flaws (ASDEX Upgrade Team) "*Stochastic sawtooth reconnection in ASDEX Upgrade.*" Biennial Workshop Stochasticity in Fusion Plasmas (Jülich, Germany, March 5-7, 2007)

2. O. Dumbrajs, V. Igochine, and H. Zohm, (ASDEX Upgrade Team) "*Diffusion in a stochastic magnetic field in ASDEX Upgrade.*" Biennial Workshop Stochasticity in Fusion Plasmas (Jülich, Germany, March 5-7, 2007)

3. D. Constantinescu, O. Dumbrajs, V. Igochine, and B. Weyssow "*On the accuracy of some mapping techniques used for the study of the magnetic field in tokamaks.*" Biennial Workshop Stochasticity in Fusion Plasmas (Jülich, Germany, March 5-7, 2007).

4. O. Dumbrajs, K.A. Avramides, and B. Piosczyk. "Mode competition in the 170 GHz coaxial gyrotron cavity for ITER" 32nd International Conference on Infrared, Millimeter, and Terahertz Waves, Cardiff, UK, September 2 -7, 2007.

5. O. Dumbrajs, K.A. Avramides, and B. Piosczyk. "Mode competition in the 170 GHz coaxial gyrotron cavity for ITER" 32nd International Conference on Infrared, Millimeter, and Terahertz Waves, Cardiff, UK, September 2 -7, 2007.

6. O. Dumbrajs, Z.C. Ioannidis, and I.G. Tigelis. "Wideband continuous frequency tunable coaxial gyrotron oscillators" 32nd International Conference on Infrared, Millimeter, and Terahertz Waves, Cardiff, UK, September 2 -7, 2007.

7. P.V. Vladimirov, V.A. Borodin, A. Möslang, A.I. Ryazanov, E.A. Kotomin, Yu.F. Zhukovskii, "Modelling of yttrium oxide particle precipitation in iron". 13th International Conference on Fusion Reactor Materials ICFRM-13 (Nice, France, December 2007), Abstracts: p. 3711.

7.2 Fusion Technology

7.2.1 Publications in scientific journals

1. J. Tiliks, G. Kizane, A. Vitins, E. Kolodinska, E. Rabaglino, "Magnetic field effects on tritium release from neutron-irradiated beryllium pebbles", Nucl. Technol. **159**, 245-249 (2007).

2. A. Vitins, G. Kizane, J. Tiliks, J. Tiliks Jr., E. Kolodinska, "Tritium release from breeding blanket materials in high magnetic field", Fusion Eng. Des. **82**, 2341-2346 (2007).

3. J. Tiliks, G. Kizane, A. Vitiņš, E. Kolodinska, V. Tilika, B. Leschinskis, "Tritium sorption and desorption from JET beryllium tiles under temperature, electron radiation and magnetic field", poster PS4-2010 presented at ISFNT-8, submitted as ISFNT-8 paper #94 for Fusion Eng. Des.

7.2.2 Conference articles

1. J. Tiliks, G. Kizane, A. Vitiņš, E. Kolodinska, B. Leschinskis. "Tritium sorption and desorption from fusion reactor plasma facing materials". – In the book: Institute of Solid State Physics. University of Latvia. Abstracts of the 23rd Scientific Conference, dedicated to commemoration of 75 years of Professor Ilmars Vitols. / Ed. by A. Krumins. – Riga, February 13-15, 2007. – P. 49.

2. J. Tiliks, V. Tilika, G. Kizane, B. Leschinskis, A. Vitins, A. Actins. "Tritium breeding ceramic pebbles synthesized from nanopowders". – In the book: International Baltic Sea Region Conference "Functional materials and nanotechnologies 2007 (FM&NT-2007)". Book of Abstracts. Riga, April 2-4, 2007. – Institute of Solid State Physics, University of Latvia, Riga, 2007. – P. 21

3. E. Kolodinska, I. Reinholds, M. Pjuse. "Investigation methods of tritium chemical forms in metallic beryllium materials". – In the book: The International Research Conference for Students. Chemistry and Chemical Technology 2007. Vilnius, Lithuania. 27th April, 2007. Abstracts. ISBN 978-9955-33-003-5. – Vilniaus Universitetas, Vilnius, 2007. – Pp. 20-22.

4. J. Tiliks, G. Kizane, A. Vitins, E. Kolodinska, V. Tilika, B. Leschinskis. "Tritium release from beryllium materials under the real operation conditions." – In the

book: The 8th International Symposium on Fusion Nuclear Technology (ISFNT-8), Heidelberg, Germany, Sept. 30 – Oct. 5, 2007. Book of Abstracts. – P. 212. The book of abstracts is available online at <http://iwrwww1.fzk.de/isfnt/boa-isfnt-8.pdf>.

5. G. Kizane, J. Tiliks, A. Vitins, E. Kolodinska, A. Supe, B. Leschinskis. "Detritiation of Be materials under action of temperature, radiation and magnetic field". – In the book: The 8th IEA International Workshop on Beryllium Technology (BeWS-8), Lisbon, Portugal, December 5-7, 2007. Book of Abstracts. – P. 17. The book of abstracts is available online at <http://iwrwww1.fzk.de/bews-8/BoA-BeWS8.pdf>.

7.3 General Articles

7.4 Doctoral and Graduate Theses

Elina Kolodinska "Tritium release from beryllium materials of thermonuclear reactors" (Master's Thesis at University of Latvia, in Latvian).